Project Report
On

Modeling and simulation of gas-liquid interfacial area in three phase fluidized and semi-fluidized bed

Under Guidance of

Prof (Dr.) G.K.Roy

And

Mr. Jiten Chandaria
(Flowmaster India Pvt Ltd)

Submitted by
Deepak Moghekar
Roll No- 20500001

Department of Chemical Engineering
National Institute of Technology, Rourkela
Rourkela-769008, Orissa

Department of Chemical Engineering

Certificate

This to certify that the Project Report titled "Modeling and simulation of gas-liquid interfacial area in three phase fluidized and semi-fluidized bed" has been done under my guidance and is a bonafide record of work done by Mr.Deepak Moghekar during session 2006-08

Date:

(Dr G.K.Roy)
Professor
Department of Chemical Engineering
National Institute of Technology
Rourkela-769008

ACKNOWLEDGEMENT

I take this opportunity to express my deep regards and sincere gratitude for the valuable, expert guidance rendered to me by guide Prof.(Dr.) G.K.Roy, Professor, Chemical Engineering Department, National Institute of Technology, Rourkela. I consider myself fortunate to have had opportunity to work under his guidance and enrich myself from his vast knowledge, and analysis power. He will always be a constant source of inspiration for us. I also sincerely thank my co-guide Mr.Jiten Chandaria, Project manager Flowmaster India Pvt. Ltd, Pune for his valuable suggestion in my endeavor.

My sincere thanks are to Dr.K.C.Biswal , Professor and Head, Chemical Engineering Department, National Institute of Technology Rourkela for his talented advice and providing necessary facility for our work.

I am also very thankful towards Dr.S.K.Agarwal Professor and PG Coordinator, Chemical Engineering Department for helping in our work. Last but not the least I am thankful to all my friends without their support this Work would not have been possible.

Deepak Moghekar

(Roll No-20500001)

M Tech. Fourth Semester

Chemical Engineering

1 Introduction

1.1. Three phase systems:

Three phase systems are vital part of chemical industry, as reactions involving gas, liquid solid are often encountered in chemical process industry [Yatish Shah 2000]. The most common occurrence of this type of three phase systems is in hydro processing industry in which variety of reactions between hydrogen and oil phase and solid catalyst have been found. The other common three phase reactions are catalytic oxidation and hydration reactions

These and other numerous similar gal-liquid–solid reactions are carried out in reactors. The three-phase system is subcategorized as

- Reactions where the gas, liquid and solid are either reactants or products
- Gas-Liquid reactions with solid as a catalyst.
- Two reaction phases and third as inert phase.
- All three phases are inert as found in unit operations.

Examples of first two types can be found very often in chemical process industry, as each phase is essential in the reaction mechanism. In the third type, one inert phase in especially added to get the advantage of three-phase system. The third inert phase induces better momentum exchange between the phases, helps in better distribution of reactant species and good temperature control. The filtration operation can be example of fourth type of three phase system

Selection and design of reactors is one of the main parameter in the performance of three phase system. As three phase system is highly complex and the success of three phase system is essentially dependent on the effective contact of each phases with other, various reactors and phase contactors were studied and operated successfully. These are three phase fixed and fluidized bed reactors, three phase semi-fluidized beds, slurry bubble columns and common CSTRs. In the recent years the three phase fluidized and semi-fluidized bed are increasingly used in three phase systems as they overcome some inherent drawbacks of fixed beds and common CSTRs.

1.2 Three phase fluidized bed:

Three phase fluidized beds are contactors in which the solid practices are fluidized by the upward moving gas and liquid phase flows. The net gravitational force on the particles is balanced by the drag force of the upward moving fluids hence the solid particle flows freely and behaves as fluid.

Gas-liquid-solid fluidization is classified mainly in four modes of operation. These are co-current three phase fluidization with liquid as continuous phase (mode I-a); co-current three phase fluidization with gas as continuous phase (mode I-b); inverse three phase fluidization (mode II-a) and fluidization represented by turbulent contact absorber (mode II-b). Modes II-a and II-b can be achieved by countercurrent flow of liquid and gas. Amongst these the most striking is co-current gas-liquid-solid fluidization with liquid as continuous phase.

The co-current gas-liquid-solid fluidization ids defined as an operation in which bed of solid particles is suspended in upward flowing gas/liquid media due to net

gravitational force on particle. Such an operation creates considerable intimate contact among the gas, liquid and solid particles and provides substantial advantages for application in physical, chemical and bio-chemical process involving gas-liquid and solid phases[1]

In conventional three phase fluidized bed, initially the solid rests on the porous grid provided at the bottom. Liquid, which is continuous phase, is introduced from the bottom of fluidized bed. The gas is introduced through the sparger introduced at the bottom. As the fluid velocity is increases gradually, the solid starts fluidizing. The liquid velocity at which solid particles first start fluidizing is called minimum fluidizing velocity. The minimum fluidizing velocity is function of solid particle density, their size and shape. The discontinuous gas phase exchanges momentum with the liquid phase and solid particles and helps in fluidization

The three phase fluidized beds are increasingly used as they overcome some inherent drawback of conventional reactors and add more advantages. The major advantages of these reactors are, they give better flexibility of mixing, heat recovery and temperature control. The three phase fluidized bed offers better gas phase distribution creating more gas-liquid interfacial area, which is vital in gas-liquid reaction system. They allow use of fine catalyst particles, which minimizes the intra-particle diffusion. Smaller is the particle larger is surface area which enables more intimate contact of phases and enhances the rector performance. These reactors can effectively be used for the rapidly deactivating catalyst and three phase reactions where solid is catalyst and also solid is used as reactant (e.g. catalytic coal liquefaction). The better mixing and high turbulence in these reactors prevents the formation of local hot spots. Potentially high reaction rate per unit reactor volume can be obtained through these reactors. Bubbling and circulating fluidized bed systems are becoming an increasingly important technology for the power generation, mineral and chemical processing industries. Benefits in economic, operational and environmental terms can be achieved with fluidized bed technology over more traditional technologies [2]

1.3 Three phase semi-fluidized bed:

A semi-fluidized bed, which is characterized by a bottom fluidized bed and a top packed bed in series within a single contacting vessel, is formed when a mass of fluidized particles is compressed by fluids with a porous retaining grid. The internal structure of a semi-fluidized bed can easily altered to create an optimal operating configuration. This unique feature of semi-fluidized bed allows it to be utilized for a wide range of physical, chemical and biochemical applications [34].

Semi-fluidization is a novel fluid solid contacting technique. The phenomenon of semi-fluidization was first reported in the subject, which was concerned with the mass transfer in the semi-fluidized bed in the liquid solid system [35]. In the conventional semi-fluidized bed, the upward moving gas-liquid fluids firstly fluidize the solids. As the fluid superficial velocities increases the solids starts expanding along the length of column. As the porous grid is provided at some distance from the bottom grid, the solids are retained at grid and further expansion is prevented. The velocity at which the solid particle first touches the top grid is called minimum semi-fluidization velocity. With further increase in fluid superficial velocities the height of

top packed bed increases. The height of top packed bed is function of gas and liquid superficial velocity, solid particle diameter, solid particle density and initial solid holdup in the column.

The semi-fluidized bed is characterized by high pressure drop. It is found that the bed pressure drop increases with both liquid and gas superficial velocity. If the liquid is continuous phase then, the minimum liquid semi-fluidization velocity decreases with increase in gas superficial velocity

Fan and Hsu have broadly stressed the application of semi-fluidized beds. Semi-fluidized beds finds wide applications as reactors for exothermic and bioreactors, in ion exchange and in filtration operation for the removal of suspended particles from gases or liquid [36]. The semi-fluidized bed provided large gas-liquid interfacial area than other reactors making it very useful for the reaction systems where rate of reaction is controlled by the gas to liquid mass transfer. The semi-fluidized bed can extensively used when the solid particles are acting as catalyst

1.4 Importance of gas-liquid interfacial area in three phase fluidized and semi-fluidized bed:

The successful design and operation of a gas-liquid-solid fluidized and semi-fluidized bed system depends on the ability to accurately predict the fundamental characteristics of the system. Specially, the hydrodynamics, the mixing of individual phases, and the heat and mass transfer characteristics [37]. Especially for multiphase reaction systems the knowledge of mass transfer and interfacial mass transfer area is vital for reactor design. The gas-liquid reaction system in which the rate of reaction is controlled by the gas side mass transfer coefficient, the gas-liquid interfacial area plays crucial part in the success of reaction system. For such system high gas-liquid interfacial area is required to obtain reasonably high rate of reaction. The gas phase exchanges heat and momentum with the surrounding through the gas-liquid interfacial area so determination of interfacial area is very important to predict the behavior of three-phase system.

Ryszard Pohorecki [28], in his communication explained the effectiveness of interfacial area for mass transfer in two-phase flow in micro reactors.

2 Literature Survey

Various methods have been adopted for determination of mass transfer coefficients and interfacial mass transfer area. Weiguo Yang et al [1] successfully studied mainly gas-liquid interfacial area and mass transfer in three phase circulating fluidized bed. They used a fiber optic probe system for measuring the bubble behavior in multiphase flow which is shown in Fig.2. The probe consists of two parallel communication optic fibers. The local gas holdup, bubble size distribution, and bubble rise velocity in different radial positions were measured using a fiber optic probe, and the effects of operating conditions on bubble rise velocity are also investigated.

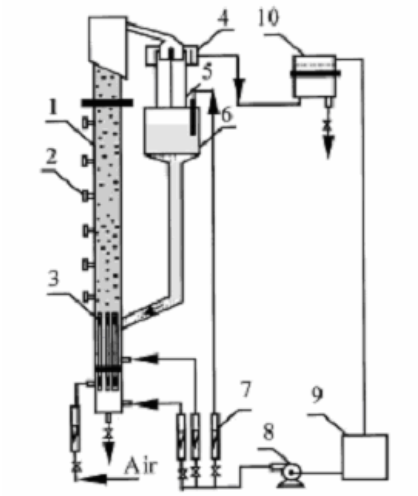

Fig. 1 Schematic diagram of experimental setup. 1- riser; 2- pressure tap; 3- gas-liquid distributor; 4- liquid solid separator; 5-particle metering tank; 6- particle reservoir; 7- flow meter; 8- liquid pump; 9- liquid reservoir; 10- secondary liquid solid separator.

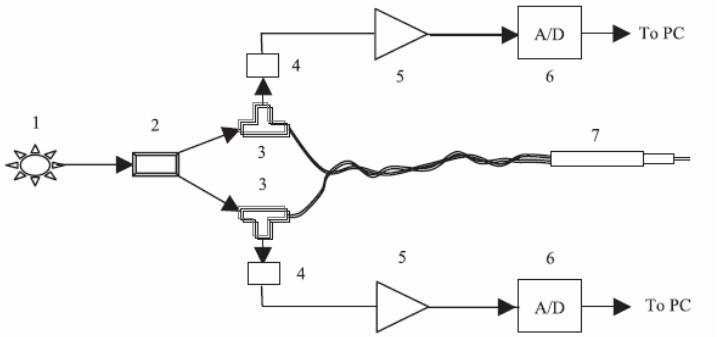

Fig.2. Hardware structure of Fiber optic; 1- laser source; 2- Light splitters; 3- Fiber coupler; 4- Light detector; 5- Amplifier; 6- A/D Transducer; 7- Probe.

The results from work of Weiguo Yang and co researchers shows that there is increase in bubble rise velocity with respect to increase in gas superficial velocity and

there is maximum flow of gas bubbles at the center of the column. They found that there is increase in gas holdup with increase in gas superficial velocity.

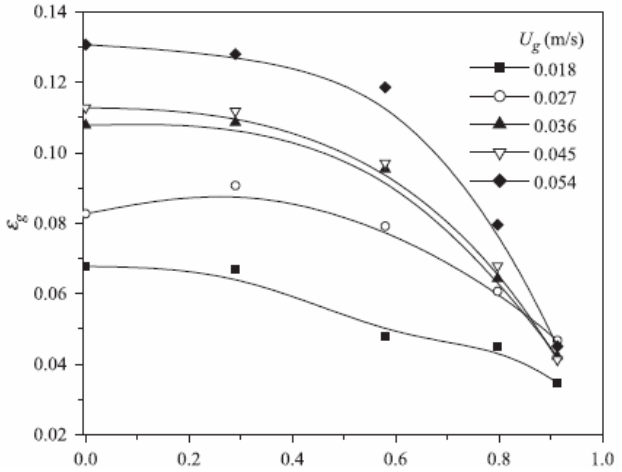

Fig.3.Radial profile of gas holdup under different Ug. (Ul1 =0.054 m/s Ul2 = 0.018 m/s, Gs = 0.072 kg/m2/s, ε_s = 0.137).

Jiasen Song.et.al [2] successfully studied the hydrodynamics and mass transfer in a three-phase fluidized bed system. They used radioactive particle tracking (RPT) to study the particle dynamics in three-phase fluidized bed. Solid-liquid mass transfer measurements were performed using a benzoic acid particle on a flexible tether. But there is always suspect that the tethered particle may not behave the same way as the free particles in three phase fluidized bed. The solid particle track report is shown in Fig.5 below.

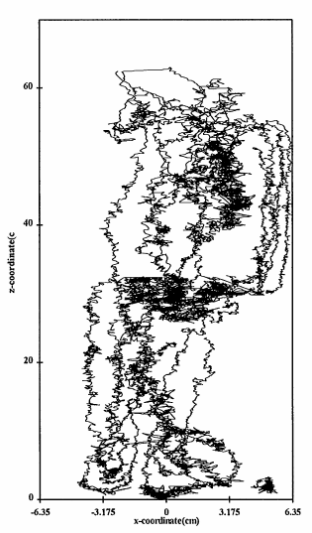

Fig.4. Schematic of *x*- and *z*-positions of tagged particle in RPT experiments at U_g 1.46cm/s;U_l 2.08 cm/s.

Sang Done Kim and Yong Kang [31] had great overview of heat and mass transfer in three-phase fluidized-bed reactors. They examined the heat and mass transfer characteristics in three-phase fluidized beds to provide prerequisite knowledge for reactor design. The effects of gas and liquid velocities, solid and liquid properties on the heat and mass transfer coefficients in three-phase fluidized beds were studied. The various correlations and models to predict the heat and mass transfer coefficients in the literature were examined and the unified correlations based on the concepts of surface renewal theory and energy dissipation rate in the beds were proposed.

L S. Fan. et .al [14]studied the effect of high pressure on bubble formation dynamics and gas holdup in three phase fluidized bed. Two-dimensional simulations of the behavior of bubble formation from multi-orifices in liquids and liquid–solid suspensions were conducted at high pressures up to 19.4 MPa under constant gas flow conditions. A discrete phase simulation (DPS) was conducted to investigate multi-bubble formation dynamics in gas–liquid–solid fluidization systems. A numerical technique based on computational fluid dynamics (CFD) with the discrete particle method (DPM) and volume tracking represented by the volume-of-fluid (VOF) method was employed for the simulation. A bubble-induced force (BIF) model, a continuum surface force (CSF) model, and Newton's third law were applied to account for the couplings of particle–bubble, bubble–liquid and particle–liquid interactions, respectively. They found that the liquid flow dynamics induced by adjacent bubbles and bubble wake significantly affects the multi-bubble formation process. The research work done by them indicates that an increase in system pressure or gas density significantly reduces the initial bubble size. Under constant flow conditions, however, the effect of pressure on the initial bubble size was insignificant.

Yong Li, Jianping Zhang and Liang-Shih Fan [22] found a numerical simulation of gas-liquid -solid fluidization systems using a combined CFD-VOF-DPM method specialy studing the effect of bubble wake behavior. A new approach that can predict the characteristics of discrete phases of three-phase flows is provided in this study. In this model, the gas-liquid-solid flow in a fluidized bed is simulated by a combined method of the computational fluid dynamics (CFD) with the discrete particle method (DPM) and a volume tracking represented by the volume-of-fluid (VOF) method. A computational model for the gas-liquid-solid three-phase fluidization system and a two-dimensional code were developed.

P.J. Witt. et.al (1998) [32] developed a numerical model for predicting bubble formation in a 3D fluidized bed. The model uses a multiphase Eulerian technique to predict the transient behavior of fluidized bed systems. The commercial CFD code CFX was used as the computational framework for solving the discretized equations. The model is used to predict isothermal flow in a three-dimensional bubbling fluidized bed. Predictions of the three-dimensional model showed bubble formation with gas bubbles or voids preferentially moving along the centre of the bed.

Yang et al. (2000) investigated the mechanism of bubble formation in liquid–solid suspensions at elevated pressures. It is found that the presence of particles increases the initial bubble size for both constant flow and variable flow.

Marmur and Rubinw developed a mechanistic model to account for the bubble formation process from a single orifice submerged in an inviscid liquid. Pinczewskiw and

Terasaka and Tsuge used the modified Rayleigh equation to predict the bubble growth rate, formation time and pressure fluctuation in the chamber under different pressures.

Luo et al (1998). and Yang et al (2000) developed analytical models to account for the initial bubble size in high-pressure liquid–solid suspensions under various bubble formation conditions. The models took into account various forces induced by particles, such as the suspension inertial force and particle–bubble collision force. Most of these models are based on the spherical symmetry assumption, and their extension to non-spherical bubble formation is unsuitable.

S. Grevskott, B.H. Sannaes et.al (1996)[12] studied liquid circulation, bubble size distributions, and solids movement in two and three-phase bubble columns. They specially worked on bubble size distribution, liquid circulation and solids movement. For the solids movement, the CARPT technique was used. By numerical simulations using a two fluid model, new models for bubble size distribution and solids presence was tested. The new bubble size model was found to improve the size distribution predictions compared to prior models. It was concluded that in order to obtain a satisfactory description of bubble size distributions in bubble columns, a model based on local conditions alone is inadequate. A population balance based model taking into account coalescence and breakup mechanisms must be implemented.

Jinghai Li, Mooson Kwauk (2003) [20] originally developed the EMMS model for two-phase system. The multi-scale methodology has received more and more attention in recent years. There are three kinds of multi-scale methodology: descriptive for distinguishing the phenomenological difference of structures at different scales; and correlative for formulating phenomena at higher scales by analyzing the mechanisms at lower scales; and variation for revealing the dominant mechanisms of the structure and the relationship between the scales. The variational multi-scale methodology consists of the following steps:

- Phenomenological resolution with respect to scales of structures.
- Identification of dominant mechanisms.
- Establishment of conservation conditions with respect to different scales and correlation between different scales.
- Formulation of variational criterion to identify what dominates the stability of structure and what compromise exists between different dominant mechanisms.
- Integration between conservation conditions with stability conditions.

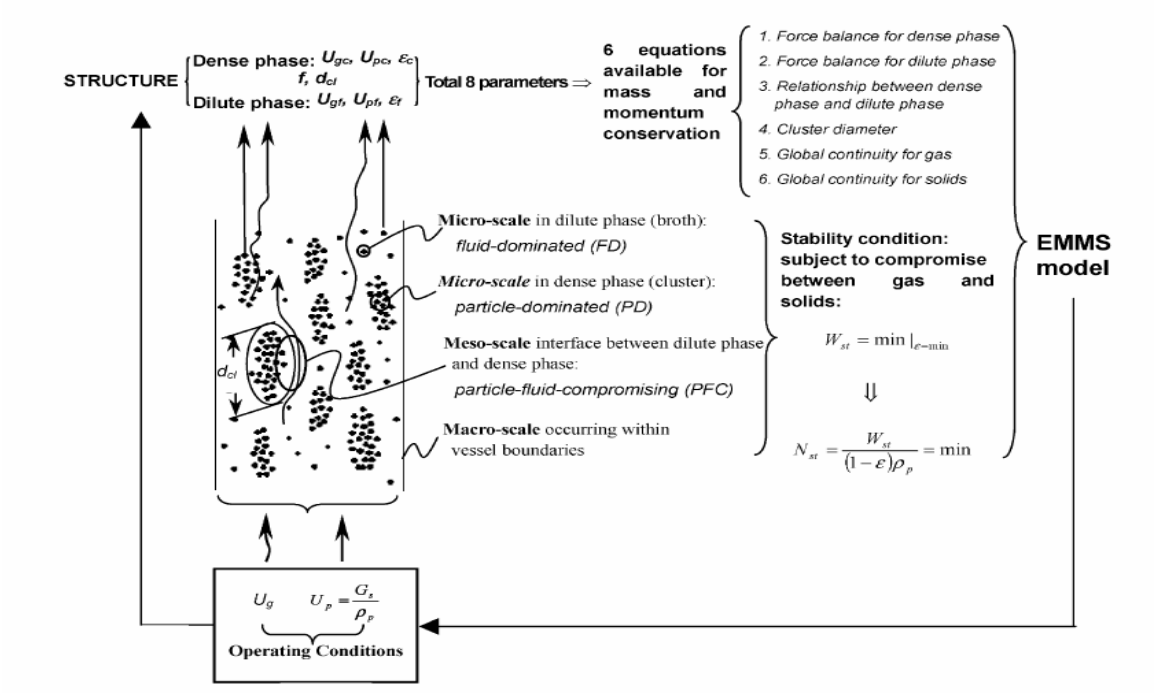

Fig 5. EMMS model for two phase system

Wei Ge [11] studied analytical multi-scale method for multi-phase complex systems. Multi-scale spatio-temporal structures, the dominant feature for all complex systems, were identified and discussed as a common challenge and frontier in process engineering, as well as in science and technology of many different fields and disciplines. Emphasis was paid to the correlation between different scales. The energy minimization multi-scale (EMMS) model for particle–fluid flow was revisited as an implementation of the analytical multi-scale method to elucidate its principles, in which the correlation between scales was established by analyzing the compromise between dominant mechanisms. They concluded that, the multi-scale method is a reasonable approach to complex systems that bridges reductionism and holism.

Jinghai Li et.al [19] developed the EMMS model for circulating fluidized beds (CFB) The model is capable of predicting the saturation carrying capacity and the steady states at both the top and the bottom of an S-shaped axial profile. Comparison between the model prediction and available experimental data shows reasonable agreement.

Jiayuan Zhang Wei Ge and Jinghai Li [24] studied simulation of heterogeneous structures and analysis of energy consumption in particle–fluid systems with pseudo-particle modeling The mass specific energy consumption *Nst* for suspending and transporting the solids is obtained by a weighted average method simultaneously. The stability criterion, *Nst* =min, proposed in the energy-minimization multi-scale (EMMS) model is demonstrated numerically, which reflects the spatial and temporal compromise of the movement tendencies of the fluid and solid phases, and leads to the formation of heterogeneous structures. When the total mass specific energy consumption for the solids (*NT*) is variable, *Nst/NT* = min should be used as a more general expression of the original stability criterion. Analysis of simulation results also shows dilute-to-dense phase drag responsible for the difference between *Nst* and *NT*. Numerical results with constant fluid flow velocity give a good proof of the original stability criterion of the

EMMS model: *Nst* = min. The simulations also demonstrated that a particle–fluid system at constant pressure drop, where *NT* is variable, is most stable when *Nst/NT* = min, which corresponds to distinct heterogeneity.

Guangwen Xu and Jinghai Li (1998) [9] developed the analytical solution of the energy minimization multi-scale model for gas-solid two-phase flow. To avoid complicated computation, analytical solution of the energy-minimization multi-scale (EMMS) model for heterogeneous particle-fluid two-phase flow was derived through analyzing the suspension properties of clusters, thus allowing local hydrodynamics, choking velocity and saturation carrying capacity to be conveniently calculated without recourse to complex mathematical algorithm. It not only greatly simplified the formulation of the EMMS model but also made the computation of the model converge more easily to its solution, and therefore greatly facilitates the application of the EMMS model.

Mingyan Liu, Jinghai Li and Mooson Kwauk [10] extended the energy-minimization multi-scale method to gas–liquid–solid fluidized beds. The three-phase fluidization system is resolved into the suspending and transporting subsystem and the energy dissipation subsystem, and the former is further divided into three sub-subsystems: liquid–solid phase, gas phase and inter-phase. Force balance is analyzed at three different scales: micro-scale of particles, meso-scale of bubbles and macro-scale of the whole system. In addition to the analysis of multi-scale interactions, the energy consumption in the system is analyzed to establish the stability condition for the system, which is considered indispensable due to the multiplicity of three-phase fluidized beds. The total energy of the system consumed with respect to unit mass of particles is resolved into two portions: suspending and transporting energy and dissipated energy. The stability condition is reached when the suspending and transporting energy of the system, Nst, is at its minimum. The model first formulated as a nonlinear programming problem consisting of six variables and seven constraints, is solved by using the general reduced gradient (GRG) algorithm. The calculated results show that the stability condition, Nst = min, can be stated alternately as db =db max. Thus, the model is finally simplified to a set of nonlinear algebraic equations.

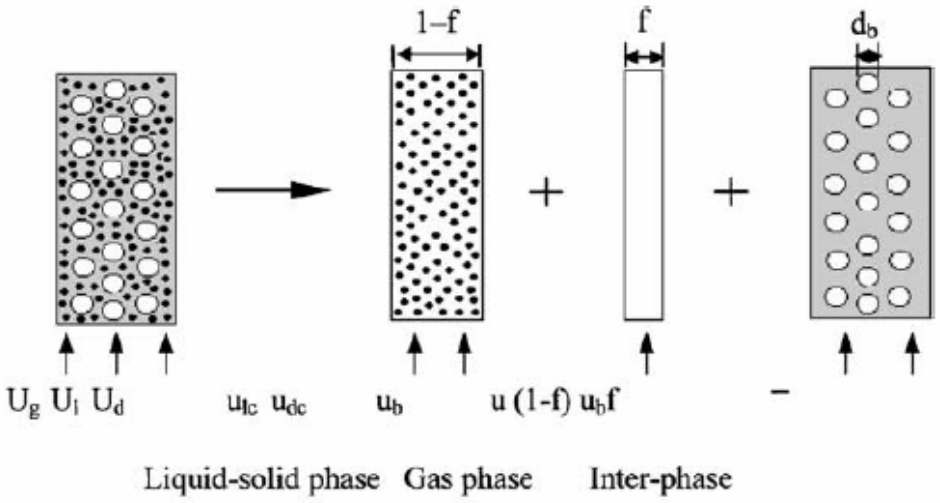

Fig.6. Resolution of suspending and transporting subsystem of gas–liquid–solid fluidization system.

Studies of semi-fluidization have been mainly limited to the gas-solid or liquid-solid systems (Fan and Wen, 1961, Babu Rao and Doriaswamy, 1970, Murthy and Roy, 1986) [31] [32][33]. A little information however is available on semi-fluidization in the gas-liquid-solid systems. G.K.Roy and Sengupta studied the design part of semi-fluidization in two-phase systems. Investigation on the hydrodynamic behavior of the inverse gas-liquid-solid semi-fluidized bed where the liquid is continuous phase was done by Chern et al. A mathematical model was proposed to account for the pressure drop in the inverse gas-liquid-solid semi-fluidized bed. Hydrodynamic study on cocurrent gas-liquid solid semi-fluidization with liquid as the continuous phase was done by Fan et al. A separate investigation was performed on a packed bed and a fluidized bed under gas-liquid flow conditions similar to that of the fluidized bed. Parameters like pressure drop, gas holdup, onset liquid velocity for semi-fluidization, and the height of the packed bed section and fluidized bed section were studied by them. Almost no work has been done on interfacial area and mass transfer in three-phase semi-fluidization.

3 Experimental Hydrodynamic work

Experiments are conducted to examine the hydrodynamic behavior viz. the pressure drop, minimum fluidization, bed expansion and phase hold up of a co-current gas-liquid-solid three-phase fluidized bed using liquid as the continuous phase and gas as the discontinuous phase.

3.1 Fluidized bed:

A schematic diagram of the experimental setup for fluidized bed is shown in Figure-7. The vertical Plexiglas fluidizer column is of 100 mm ID with a maximum height of 2m.The column consists of three sections, v.i.z., the gas-liquid disengagement section, test section, and gas-liquid distributor section. The gas-liquid distributor is located at the bottom of the test section and is designed in such a manner that uniform distribution of the liquid and gas can be maintained in the column. The distributor section (Figure-9) is a conical frustum of 12 cm in height, one end 5.08 cm in diameter and the other end of 10 cm diameter having liquid inlets one of 24 cm ID with a perforated plate (Figure-8) made of G.I. sheet of I mm thick, 120 mm diameter, of about 278 numbers of 2, 2.5 and 3mm pores in placed at the top of this section. There is a gas distributor consists of 50 numbers of 1mm pores placed randomly. In this section the gas and liquid streams merged and passed through the perforated grid. The mixing section and grid ensure that the gas and liquid are well mixed and evenly distributed into the bed. Gas-Liquid Disengagement Section is at the top of the column, which allows gas to escape and liquid to be circulated. Any entrained particles retain on the screen attached to the top of this section. For pressure drop measurement the pressure ports are being fitted to the U-tube manometers of 1m & 0.5m long filled with mercury and carbon tetrachloride.

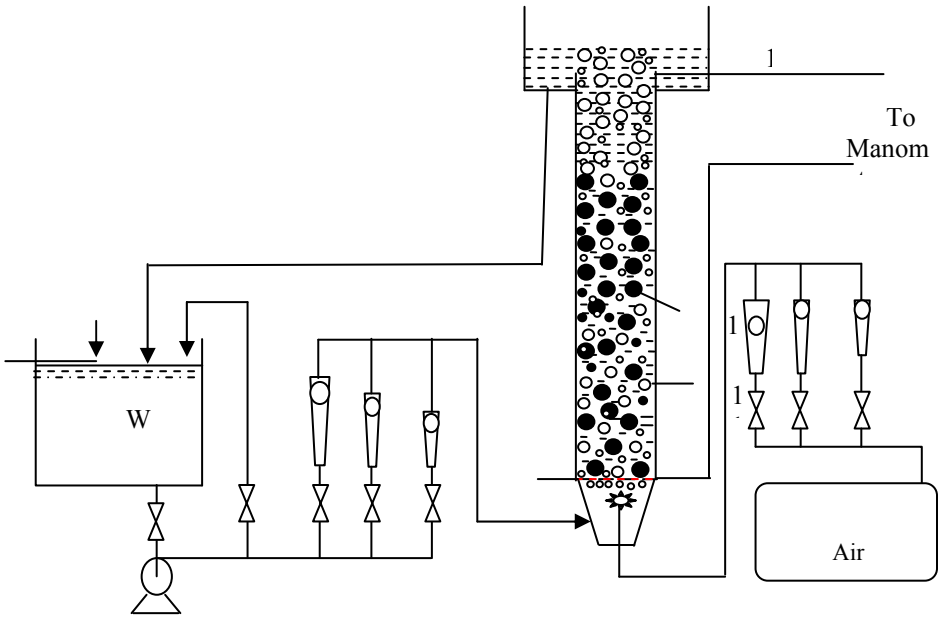

1-Gas-liquid disengagement section
2-Test section
3-Gas-liquid distributor section
4, 5-Rotameters
6-Quick closing valves
7-Liquid pump
8- Air sparser
9-Bottom grid
10- solid particles
11-Air bubbles

Fig.7: Schematic diagram of gas-liquid-solid three-phase fluidized bed

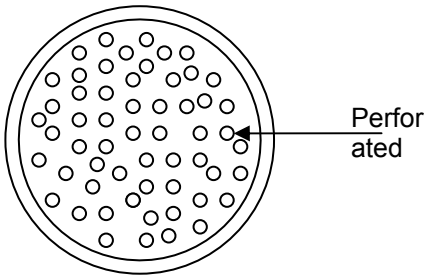

Fig 8: Schematic diagram of the gas and liquid distributor**.**

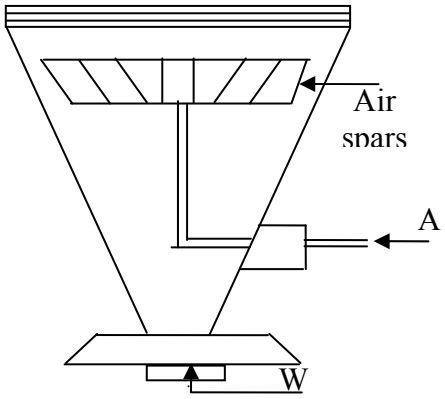

Fig 9: Schematic diagram of conical calming section**.**

Through hydrodynamic study of fluidized bed is performed. Experiments are done to study the pressure drop, minimum fluidization velocity with respect to variation in solid holdup, gas and liquid superficial velocity. Particle of different diameter and different density were tried and hydrodynamic results are obtained. Gas and liquid superficial velocities are varied over a broad range to check their effect on hydrodynamic behavior of fluidized column. The results obtained from hydrodynamic study were used as inputs for modeling and CFD analysis of gas-liquid interfacial area.

3.2 Semi-fluidized bed:

A schematic diagram of the experimental setup for SEMI-fluidized bed is shown in Figure-10.The experimental setup for semi-fluidized bed is same as that of fluidized bed with addition of top perforated grid located at some distance from the bottom grid. The position of top grid can be varied along the length of the column so at to fit the desired conditions. Experiments are done to predict the hydrodynamic behavior such as pressure drop across the semi-fluidized bed, minimum semi-fluidization velocity, rate of top packed bed formation, ratio of packed bed to fluidized bed etc. in which co-current flow of a gas and a liquid takes place in a bed of cylindrical particles with moderate density.

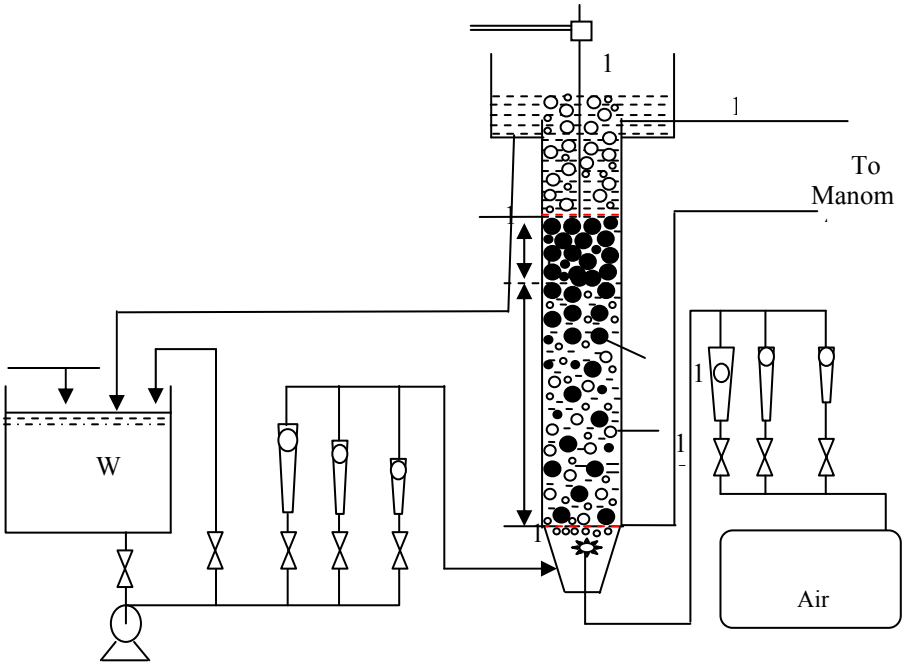

1-Gas-liquid disengagement section
2-Test section
3-Gas-liquid distributor section
4, 5-Rotameters
6-Quick closing valves
7-Liquid pump
8- Air sparser
9-Fluidized bed section
10-Packed bed section
11-Top screen
12-Bottom grid
13–Clam holder to freely adjust the top screen level
14- solid particles
15-Air bubbles

Fig 10: Schematic diagram of a three-phase semi-fluidized bed

4 Determination of gas-liquid interfacial area in three phase fluidized bed

Determination of gas-liquid interfacial area in three phase fluidized bed by using EMMS model:

The energy-minimization multi-scale (EMMS) method, originally developed for describing the gas–solid heterogeneous flow system by Li and Kwauk [20] and recently validated through discrete pseudo-particle approach, was extended to gas–liquid–solid three-phase flow system, however, without consideration of the effects of bubble wakes [10]. In fact, the hydrodynamics of bubble wake located immediately underneath the bubble base and rising at almost the same velocity of the bubble is totally different from that of the surrounding liquid–solid suspension. It has been specially recognized that the bubble wake is the dominating factor contributing to the intimate liquid/solid mixing and bed contraction performance [9]. In this study, the multi-scale resolution with respect to the scales of flowing structures in the three-phase flow is done with the consideration of the bubble wake effects. Simultaneously, the turbulent kinetic energy of the eddies induced by the rising bubbles and the surface energy are thought to be the dominating factors for controlling the bubble size.

Like the gas–solid fluidized systems, flows in the gas–liquid– solid three-phase fluidized beds are also characterized by structure heterogeneity and regime multiplicity due to the complex interactions between phases [20] For such complex systems, additional constraints for system stability may be indispensable in addition to those for mass and momentum conservation. On the other hand, gas–liquid–solid flow manifests its complex behavior largely at three different scales, i.e., micro-scale of solid particles, meso-scale of bubbles and bubble wakes, macro-scale of the whole bed unit with the influence of the unit boundary, and interactions also occur among these different scales. Meanwhile, the multi-scale characteristic of turbulence induced by liquid shear and rising bubbles extremely complicates the system. Solid particles have complex interaction with turbulence eddies according to particle physical properties such as particle diameter and density. Turbulences at different scales have different effects on bubble behaviors, among which the turbulence at the length scale of bubble diameter is responsible for the bubble size. Therefore, effective analysis of the interactions at different spatial scales is especially important for appropriately describing the hydrodynamics in the three-phase flow. The energy-minimization multi-scale (EMMS) method, originally developed for describing the gas–solid heterogeneous flow system by Li and Kwauk [20] and recently validated through discrete pseudo-particle approach [10], was extended to gas–liquid–solid three-phase flow system, however, without consideration of the effects of bubble wakes [10]. In fact, the hydrodynamics of bubble wake located immediately underneath the bubble base and rising at almost the same velocity of the bubble is totally different from that of the surrounding liquid–solid suspension. It has been specially recognized that the bubble wake is the dominating factor contributing to the intimate liquid/solid mixing and bed contraction performance. In this study, the multi-scale resolution with respect to the scales of flowing structures in the three-phase flow is done with the

consideration of the bubble wake effects. Simultaneously, the turbulent kinetic energy of the eddies induced by the rising bubbles and the surface energy are thought to be the dominating factors for controlling the bubble size.

4.2. EMMS model for three-phase fluidized beds:

The EMMS model, consists of the following main steps [20]:

1. Phenomenological resolution with respect to scales of structures.
2. Establishment of conservation conditions with respect to different scales and correlation between different scales
3. Identification of dominant mechanisms and formulation of variational criterion to identify what dominates the stability of structure and what compromise exists between different dominant mechanisms
4. Integration between conservation conditions with stability conditions

The EMMS model for the three-phase fluidized bed in this study is based on the above principles.

4.2.1 System resolution with respect to scales in three-phase system:

Various interactions at different spatial scales occur in the gas–liquid–solid fluidized beds, including the persistent contacting of the particles and bubbles with liquid; and collisional interactions between bubbles and particles. The following analyses are based on the main interactions in the gas–liquid–solid fluidized beds. Like the gas–solid two-phase system , the gas–liquid–solid system is resolved into a suspending and transporting subsystem and energy dissipation subsystem. Hence, the total power associated with a three-phase system, expressed as power consumed in a volume containing unit mass of solids, NT, is considered to consist of the sum of the power for suspending and transporting particles, Nst, and the one purely dissipated in particle collision, circulation, acceleration, liquid viscous dissipation$N$d, and the increase rate of surface energy due to bubble splitting Nsur (NT =Nst +Nd +Nsur). The overall flow behavior reflects the complex interactions among the individual phases at different scales.

In order to efficiently describe the most prominent interaction of solid particles with liquid, and the interaction of rising gas bubbles and their wakes with the surrounding liquid–solid mixture, the suspending and transporting subsystem is further resolved into five phases: the liquid–solid phase, the gas phase, the bubble wake phase, one inter-phase describing the interaction between the rising gas bubbles and the surrounding liquid–solid suspension and the other inter-phase describing the interaction between bubble wakes and the surrounding liquid–solid suspension as shown in Fig. 11.

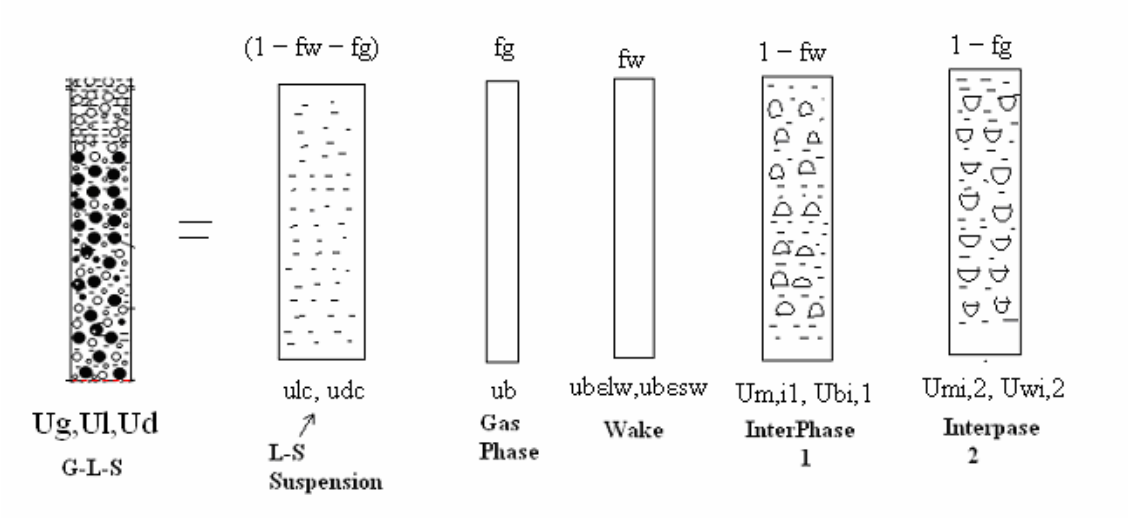

Fig.11 Resolution of transporting and suspending subsystem in three phase System

Like the generalized bubble wake model, it is assumed that the wake rises at the same velocity as that of the bubble over it. Eight variables are proposed to describe such systems, $\boldsymbol{X}$= (fg, fw, ub, $u$dc, $u$lc, εlc, εlw, db), where fg is the holdup of the bubbles, fw the holdup of bubble wakes, ub the rising velocity of bubbles and bubble wakes, $u$dc and $u$lc the superficial velocity of particle and liquid in the solid–liquid phase, εlc the liquid holdup in the liquid–solid phase, εlw the liquid holdup in the bubble wake phase and db is mean bubble diameter. As shown in Fig. 11, the interactions occurring in different phases are micro-scale of particles, meso-scale of bubbles and bubble wakes, and macro-scale of the whole bed unit, respectively. Micro-scale interaction is concerned with the interaction between individual particles and the fluid surrounding them. It is assumed that no particles are present in gas bubbles, and solid particles and liquid contained in a bubble wake rise at the same velocity as the bubble above it.

Micro-scale interaction only exists in the liquid–solid phase which is expressed as the balance between the drag force and effective gravity of solid particles. In the liquid–solid phase, the particles are assumed to be uniformly suspended, and the dilute–dense two-phase structure and thus the energy dissipation as in gas–solid system is neglected [20]. The interaction between particles and liquid in the liquid–solid phase can be described using the Richardson–Zaki relationship [24]. Meso-scale interactions are concerned with the interaction of dispersed bubbles and bubble wakes with the liquid–solid suspension. The former is expressed as the force acting on bubbles by the liquid–solid suspension through the inter-phase. The liquid–solid phase is treated as a pseudo-homogeneous mixture with the mean physical properties and averaged velocity. However, the interaction between bubble wakes and the liquid–solid phase is very complex, and it cannot be directly expressed with a simple theoretical relationship at present, thus the empirical correlations based on experiments are used to calculate the wake size and solid concentration in the primary wake. Macro-scale interaction occurs between the whole system and the boundaries such as the walls, the inlet and outlet of the bed. This macroscale interaction will not be dealt with for the moment in this study.

4.2.2 Conservation conditions at different scales:

4.2.2.1. Momentum equation for particles in the liquid–solid phase:

It is assumed that the generalized Richardson–Zaki relationship is suitable for the uniformly fluidized particles in the solid–liquid phase. This relationship implies the local balance among the gravity of particles, the buoyancy force and the drag force in unit volume of liquid–solid phase [24]:

$$u_{lc}/\varepsilon_{lc} - u_{dc}/(1-\varepsilon_{lc}) = u_t \varepsilon_{lc}^{\,n-1} \quad \text{…….. (1)}$$

where ut is the terminal velocity of the particle in a stable liquid, and it can be iteratively computed using Eqs. (2)–(4) or obtained by experimental measurement [8],

$$u_t = (4\, g\, dp\, (\rho_p - \rho_f) / 3\, \rho_f\, C_{D,p0})^{0.5} \quad \text{……(2)}$$

$$C_{D,p0} = 24/\mathrm{Ret} + 3.6/\mathrm{Re}_t^{0.313} \quad \text{…….. (3)}$$

$$\mathrm{Re}_t = \rho_l u_t dp / \mu_l$$

and n is Richardson–Zaki index, which depends on the terminal Reynolds number Ret as follows [13]:

$$\begin{array}{ll} n = 4.65 & Re_t\, t < 0.2 \\ n = 4.4\ Re_t^{-0.03} & 0.2 < Re_t < 1 \\ n = 4.4\ Re_t^{-0.1} & 1 < Re_t < 500 \\ n = 2.4 & Re_t > 500 \end{array} \quad \text{……(4)}$$

4.2.2.2 Momentum equation for dispersed bubbles in the liquid–solid suspension:

Dispersed bubbles flow through the liquid–solid suspension which is regarded as a pseudo-homogeneous fluid with a mean density ρ_m, a mean superficial velocity u_m and an effective viscosity μ_m, which are, respectively, defined as [15]

$$\rho_m = \rho_p \varepsilon_{sc} + \rho_l \varepsilon_{lc}, \quad \text{……..(5)}$$

$$u_m = (\rho_p u_{dc} + \rho_l u_{lc)} / \rho_m \quad \text{…….(6)}$$

$$\mu_m = \mu_l \exp(\varepsilon_{sc} / (1 - \varepsilon_{sc}/0.724) \quad \text{…..(7)}$$

Bubbles interact with the mixture through the inter-phase 1 in which bubble wakes are not considered, thus the gas volume fraction is corrected as fg/(1- fw) in this inter-phase. The efficient weight is balanced by the drag force of the liquid–solid suspension, thus the momentum equation for bubbles can be expressed as

$$(3/4)(1/d\mathrm{b})\, C_{D,\,b0}\, (1 - (f\mathrm{g}/1 - f\mathrm{w})^m \rho_m\, (f\mathrm{g}/1 - f\mathrm{w})(u_b - u_m)^2 = f\mathrm{g}(1 - f\mathrm{w} - f\mathrm{g})\, (\rho_m - \rho_g) g/(1 - f\mathrm{w})2 \quad \text{…(8)}$$

where$C_{D,b0}$ is the drag coefficient for a single bubble and defined as

$$C_{D,b0} = 2.7 + 24/ Re_d \quad \ldots(9)$$

Re_d is the Reynolds number with the characteristic length of the mean bubble diameter,

$$Re_d = \rho_m d_b(u_b - u_m) \ \mu_m^{-1} \quad \ldots.(10)$$

$C_{D,g0}(1-fg/(1-fw))^m$ is the drag coefficient for bubbles, including the effect of bubble swarm. m varies with the bubble terminal Reynolds number and m= 2 for large bubbles according to the drift model of Wallis.

4.2.2.3 Mean bubble wake size and particle concentration in the bubble wake:

Turbulent bubble wake is unstable and the vortex in it sheds with a certain frequency. In order to quantify the extent of the exchange or interaction of the bubble wake phase with the surrounding liquid–solid mixture in inter-phase 2, two parameters, that is, the wake holdup, fw and the particle concentration in the wake (εsw =1- εlw) should be determined. Due to the instability of the wake, the wake size is not a constant but changes continuously with time as a saw-tooth wave function. It is very difficult to directly describe the interaction between the wake phase and surrounding liquid–solid phase theoretically, several models based on experimental observation or theoretical assumption, such as the saw-tooth wave function model, the bubble wake pendulum model, Hill's spherical model and the completing spherical model were proposed to compute the mean size of the bubble wake. In this study, the relationship combining two correlations for a steady wake behind a small bubble at low gas Reynolds numbers and for an unsteady wake at higher gas Reynolds numbers according to the sawtooth wave function model is suggested to compute the mean relative size of the wake behind a single bubble ($k0 = Vw/Vb$) in the three-phase fluidized beds,

$$k0 = (200(Reb - 20)^{-1.12} + 0.24)^{-1} \quad \ldots\ldots\ldots\ldots\ldots\ldots(11)$$

Note that $Reb = b\rho_m(ub - um)\ \mu_m^{-1}$ and it is defined with a characteristic length of the major axis or width of the bubble b. It is more proper to define the gas Reynolds number due to the bubble shape transition apart from a sphere. To relate Reb with Red, the ratio of equivalent diameter db to b, db/b and the aspect ratio (minor (vertical) axis/major (horizontal) axis) h/b should quantify. The aspect ratio is a function of the Tadaki number Ta, defined as

$Ta = ReMo^{0.25}$, and

$Mo = g\mu_l^4 (\rho_l - \rho_g)/(\rho_l^2\sigma^3)$.

For ellipsoidal and spherical-cap bubbles, db/b = $(h/b)^{1/3}$, thus

$$Reb = Re_d b/d_b \quad \ldots\ldots..(12)$$

To account for the effect of gas holdup on bubble wake size, the volume fraction of bubble wake fw can be expressed as

$$fw = fgk0 \exp(-5.05fg). \quad \ldots\ldots\ (13)$$

Solid concentration in the bubble wake increases with the decrease of particle size and the increase of gas velocity and liquid viscosity. The empirical equation for the average solid holdup in the primary wake proposed by Kreischer et al. can be used

$$\varepsilon_{sw} = 0.52(Red/Ret^{)-1/8}\varepsilon_{sc}^{5/4} \quad \text{……(14)}$$

4.2. 3 Continuity equations for gas, liquid and solid:

The continuity equations for gas, liquid and solid are, respectively,

$$u_b f_g - U_g = 0, \quad \text{…….(15)}$$

$$u_{lc}(1 - f_g - f_w) + u_b \varepsilon_{lw} f_w - U_l = 0, \quad \text{…… (16)}$$

$$u_{dc}(1 - f_g - f_w) + u_b(1 - \varepsilon_{lw}) f_w - U_d = 0. \quad \text{…… (17)}$$

4.2.4. Bubble size in three-phase fluidization:

The multiple dispersed bubbles in the gas–liquid–solid system are thermodynamically unstable, however, can be maintained at a dispersed state with a mean bubble diameter due to the balance between the surface energy and the destructive turbulent kinetic energy input from the surrounding suspension. There exists a competitively dynamic process of bubble coalescence and break-up in three-phase fluidized beds. For spherical bubbles with a given gas holdup in the threephase system, the specific area $\Lambda = 6f_g/d_b$, and the specific surface energy $E_{sur} = \Lambda\ \sigma = 6\sigma f_g/d_b$ [9]. Bubble coalescence means the increase of d_b and the reducing of a, correspondingly, the reducing of the surface energy E_{sur}, bubble coalescence is thus a spontaneous tendency and the bubble diameter tends to become as large as possible through coalescence for a multiple-bubble system, leading to a minimum surface energy,

$$E_{sur} = 6\sigma f_g / d_b \rightarrow E_{sur} \text{ -> min.} \quad \text{……. (18)}$$

Meanwhile, for a given gas holdup, larger bubbles suffer a smaller resistance when they go upwards through the liquid–solid mixture. However, bubbles are dispersed and do not coalesce until two bubbles collide and contact for a certain period of time. In a three-phase fluidized bed, bubble coalescence may occur according to the mechanisms similar to those in a gas–liquid system. It is assumed that coalescence happens in three steps: first, two bubbles collide, trapping a small amount of liquid as a thin film between them. Second, the liquid drains until the liquid film reaches a critical thickness. Third, the film ruptures leading to the coalescence. Therefore, the coalescence rate is rated to two key parameters, that is, the collision rate and the collision efficiency. The collision rate may result from the large scale turbulent eddies, the buoyancy and laminar shear. These mechanisms are cumulative. The collision efficiency is a measure of what fraction of bubble collisions lead to coalescence events, and it is a function of the contact time between bubbles and the time required for bubbles to coalesce. On the other hand, the break-up of bubbles leads to the increase of specific area Λ, thus the increase of surface energy E_{sur}, additional work must be input from the surrounding suspensions. Few theories for bubble break-up in the three-phase fluidized bed are available. Except for the bubble-particle collision break-up mechanism [22], most of the theories for bubble break-up are derived from the theories proposed by Hinze [9] or Levich [9] for gas–liquid system. Large bubbles may be deformed and ruptured into smaller ones through bubble

interaction with turbulent eddies generated in the liquid. The scale of eddies responsible for break-up is equal to or a little smaller than that of the bubble diameter. Large eddies just simply transport the bubbles, resulting in random motion of bubbles without causing them break up, while very small eddies do not contain sufficient energy to cause breakage.

According to Levich's theory, the maximum stable bubble diameter $d$max is given by

$d\text{max} = (We\text{'c} / 2)^{0.6} (\sigma^{0.6} / \rho_l^{0.4} \rho g^{0.2}) \zeta^{-0.4}$

where the criticalWebber number We'c is in the range of 0.6–1.5. In practical application, the most commonly used bubble diameter is the Sauter mean diameter d3,2, which measures the ratio of bubble volume to the surface.

The mean ratio of d3,2 and db,max is [10]

$d3,2 / d\text{max} = 0.62.$ (19)

If the effect of the gas holdup on bubble size is considered, according to Levich's theory, the Sauter mean bubble diameter for the three-phase system can be expressed as

$$d_{3,2} = 1.25(\sigma^{0.6}/(\rho_m^{0.4} \rho_g^{0.2}))\zeta^{-0.4} f^{0.37} \quad (20)$$

where the local energy dissipation rate ζ is assumed to equate the rate of work done by the net buoyancy force acting on bubbles times the relative velocity of bubbles to the surrounding suspension in unit mass of liquid,

$\zeta = (f\text{g}(1 - f\text{w} - f\text{g})(\rho_\text{m} - \rho_\text{g})g (u_\text{b} - u_\text{m}) / ((1 - f\text{w})^2 \varepsilon\text{l}\rho\text{l})$ (21)

In gas–liquid–solid three-phase fluidized bed, the bubble-induced turbulence dominates over the liquid shear-induced turbulence over a broad operating range of gas superficial velocities [28]. Therefore, it is assumed that the mean size of bubbles is determined by the turbulent kinetic energy induced by the rising bubbles. The work done by the net buoyancy force of bubbles is first converted to the kinetic energy of eddies, that is, the turbulent kinetic energy in the primary wake required to maintain the vertical/circulating motion in the wake, and subsequently dissipated into the surrounding mixture as soon as part of the primary wake sheds into the secondary wake. The maximum stable bubble diameter theory provides a constraint condition for the variation of mean bubble diameter:

db <= $d3,2$. (31) The equation set including Eqs. (1), (10), (15)–(19) is the conservation conditions for the particles, bubbles and bubblewakes. The seven equations as well as the constraint condition (31) are not sufficient to determine the stable state of the gas–liquid–solid system with eight unknowns. Stability conditions for the threephase system must be provided.

4.2.5 Stability conditions for three-phase fluidized beds:

In the gas–liquid–solid fluidized bed, particles tend to maintain themselves as low as possible in the bed with minimum potential energy, leading to a maximal particle volume fraction εs -> →εs,max. The continuous liquid directly contacts particles and its drag force balances the weight of the particles immersed it. The dispersed gas bubbles do not directly contact the particles except for particle–bubble collision; bubbles directly contact liquid and transfer their momentum to liquid to fluidize particles. The fluid motion tends to consume a minimum power for transporting and suspending particles per unit bed volume, that is, Wst =Wst,l–s +Wst,gas→Wst,min. In most flow regimes, neither the particles nor the fluid can dominate the other in displaying either's tendency

exclusively, they have to compromise each other in such as way that the particles seek as much as possible minimum potential energy and the fluids (including continuous liquid and dispersed bubbles) flow through the particles as much as possible with minimum resistance, leading to the stability condition for the three-phase fluidized beds, the same as the gas–solid two-phase flow [13]:

$N\text{st} = N\text{st,l–s} + N\text{st,gas} \rightarrow$ …….. (22)

$N\text{st}$ -> min,

where Nst is defined as the power consumed for transporting and suspending particles in a volume containing unit mass of particles, $N\text{st} = W\text{st}/(\varepsilon_s \rho_p)$.

The associated correlations for Nst are given below

$NT = Nst_{l\text{-}s} + Nst_{B\text{-}LS}$

For liquid solid suspension:

The slip velocity*:* $u\text{sc} = u\text{lc}/\varepsilon\text{lc} - u\text{dc}/\varepsilon\text{sc}$

Momentum exchange coefficient: $\beta_{sc} = (\rho_p - \rho_l) g \varepsilon_{sc} \varepsilon_{lc}^{2-n} / u_t$

Drag force for particles or bubbles in unit volume $F\text{dp} = \beta_{sc} u_{sc}$

Suspending and transporting power consumed in unit volume: $W\text{st,l–s} = F\text{dp} u_{lc}$

Suspending and transporting power consumed per unit mass of particles $Nst,l–s = Wst,l–s(1 - fg - fw) / \varepsilon_s \rho_p$

Bubble/liquid–solid suspension:

The slip velocity*:* $u\text{sb} = u\text{b} - u\text{m}$

Drag coefficient for bubble $Cdb = Cdb0 (1 - fg /(1 - fw))$

Momentum exchange coefficient $\beta\text{int1} = 3 /4 C\text{D,b} (\rho\text{m}/d\text{b}) (f\text{g} / (1-f\text{w}))(u\text{b} - u\text{m})$

Drag force for bubbles in unit volume $F\text{dp} = \beta\text{int1} u\text{sb}$

Suspending and transporting power consumed per unit mass of particles $N\text{st,gas} = W\text{st,gas}(1 - f\text{w})/ \varepsilon_s \rho_p$

4.3. Validation of results:

Eight variables are proposed to describe the three phase fluidized system, $\boldsymbol{X}$= (fg, fw, ub, $u$dc, $u$lc, εlc, εlw, db), If we select one of the eight unknowns and give it a trial value in a proper range, for example, fg in the open interval (0, 1), the seven equations is closed for the other seven unknowns. For every given trial value of fg, we can solve the non-

linear equation set established in the above section iteratively, and if the solution exists, we can compute the value of objective function *N*st. For this code is written in .Net C#. The model is simulated for wide range of gas and liquid superficial velocities. The results were obtained and compared with the experimental data in the literature.

Through this method, we can know the variational tendencies of all the parameters, as well as the objective function, and search the optimal solution among all the feasible solutions. Experimental results reporter in literate by Matsuura and Fan (1984) were used as reference for comparison.

5. CFD analysis of three phase fluidized bed for gas liquid interfacial area

The modeling of fluidized bed reactors is challenging because of their complex flow behavior and the many interactions. Of the various modelling tools, computational fluid dynamics (CFD) is the most promising for future fluidized bed modelling. CFD is intended to include the key mechanisms of importance to predict accurate flow and other characteristics of fluidized beds for design, scale-up and optimization. In general, two different categories of CFD models are used for fluidized beds. The Lagrangian model solves equations of motion for each particle taking into account particle–particle collisions and the forces acting on the particle, whereas Eulerian models consider fully interpenetrating continua subject to continuity and momentum equations [19].

Most authors have used Eulerian models, including continuity and momentum equations for two interpenetrating continua, one representing the gas and the other the solid. To achieve closure, a granular temperature (energy balance) model has usually been included. When turbulent flow of the gas phase is assumed, a *k*. model is also likely to be incorporated. Different authors have utilized different assumptions with respect to such aspects as boundary conditions, interphase momentum transfer (drag) relationships, and parameters (primarily coefficients of restitution and radial distribution function) in the Eulerian model

For the CFD analysis of three phase fluidized bed geometry of the actual experimental fluidized bed setup is done in Gambit 2.3.16. The actual experimental fluidized bed column geometry is created in Gambit with height of the bed reduced to limit the cell count.

The fluidized bed column is divided into 3 zones namely the bottom distributor section, the middle part containing rest solids and top test section. This is done to take care of individual fluid domains get optimum cell number. The water i.e. liquid phase is introduced from the bottom of the column. The air is introduced through the sparger. Here sparger is developed as circular plate having thickness of 1cm. Holes of square size of 2mm are made. As the size of holes is smaller making it as circular would not had any difference. The square size holes are better for fine and good quality mesh. Only top surface of the sparger is meshed and all the other faces are considered as wall. The perforated grid at the bottom of the column, which helps n distribution of liquid and gas flow, is modeled as porous media with 25 percent opening. Good quality mesh of the porous grid is one of the main factor in the success of the CFD analysis.

The bottom distributor section is meshed as tetrahedral. The tetrahedral mesh is better but increases the cell count. So balance is to be made between the mesh quality and mesh count. The top test section is meshed as wedge mesh and cooper scheme it is converted into hexahedral. Mesh for best quality mesh. The interval size if top test section is kept at 6. The equisize sequins of the worst cell of wedge shaped in the test section is 0.33973 and that of tetrahedral cells in the distributor is 0.801137. The equisize sequins in both sections are quite lower than the permitted sequins of 1. the total cell cont for tetrahedral cells in the distributor section is 75171 and of wedge shaped cells in the test section is 32736. The total cell count for the column is 107907. The mesh is generated and boundary conditions are defined for each phase and for overall column.

The mesh file is exported from GAMBIT and imported in Fluent. The grid was checked and the mesh is converted into polyhedra. The conversion in polyhedra reduces the total cell count and improves the mesh quite a lot. The total cell count after polyhedra conversion is 41937.

The air and water are defined as velocity inlet. The outlet of the column is defined as pressure outlet with atmospheric pressure. Now the column is defined in four separate fluid zones. These are bottom distributor zone, the perforated (here porous) grid fluid zone, and the bottom test section

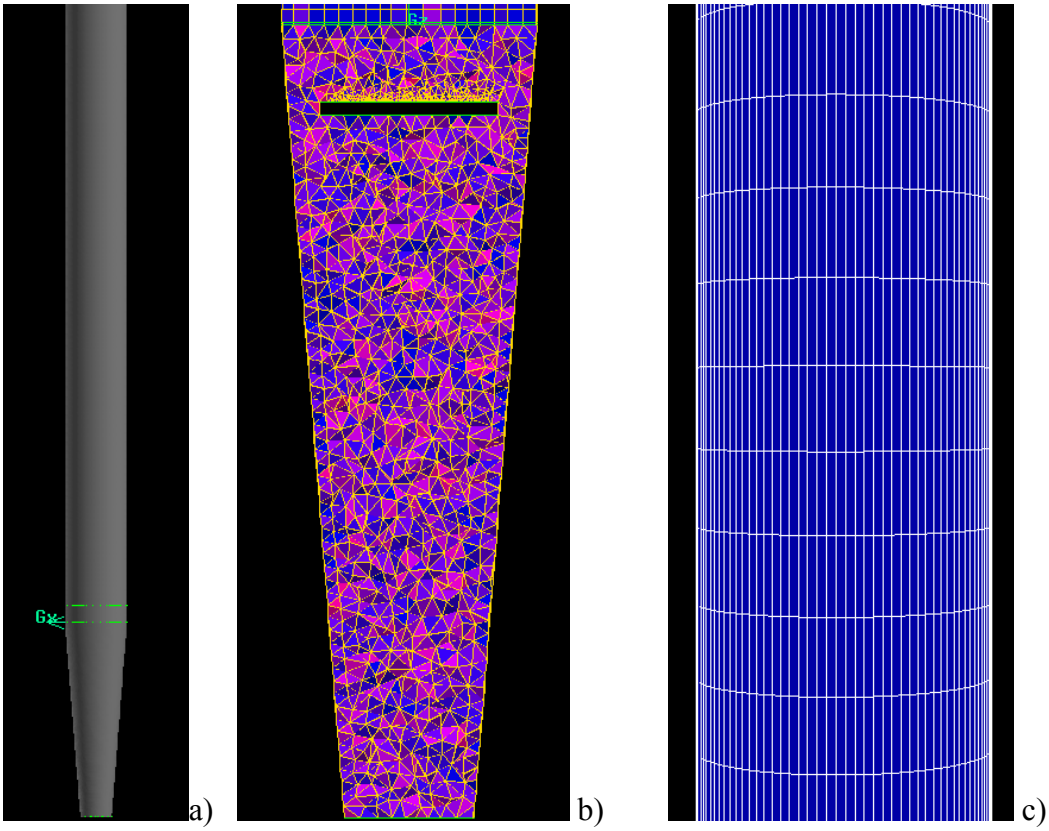

Fig.12 a) Solid geometry of fluidized bed column
Fig 12 b) Wedge mesh of bottom distributor section
Fig. 12 c) Hexahedral mesh of top test section

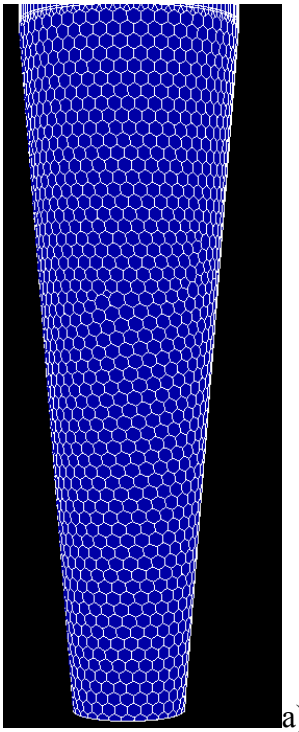
a)
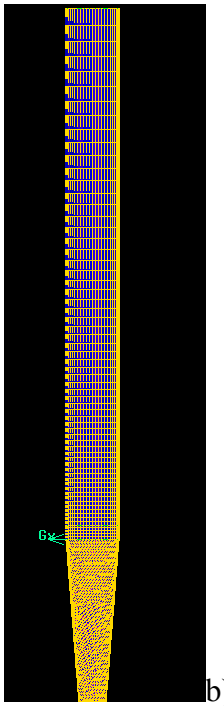
b)
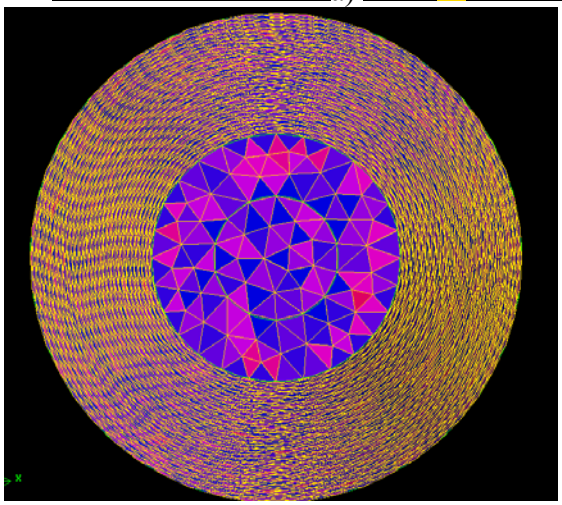
c)
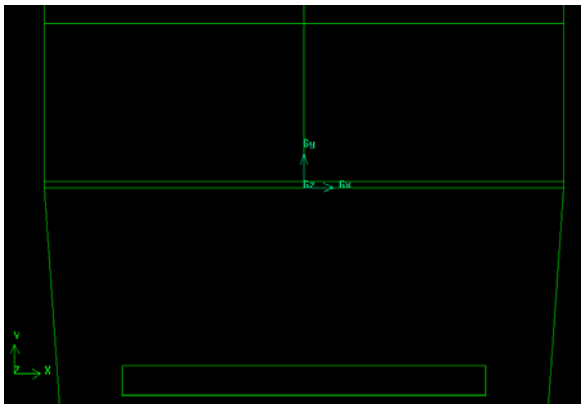
d)

Fig. 13 a) Tetrahedral meshed bottom distributor section
Fig. 13 b) Mesh fluidized bed
Fig. 13 c) Bottom view of fluidized bed column
Fig. 13 d) Bottom test section

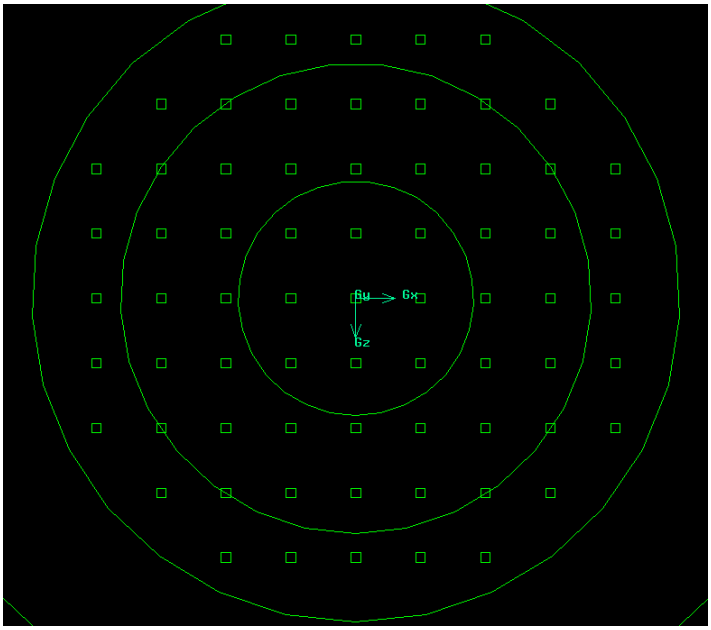

Fig. 14 The sparger

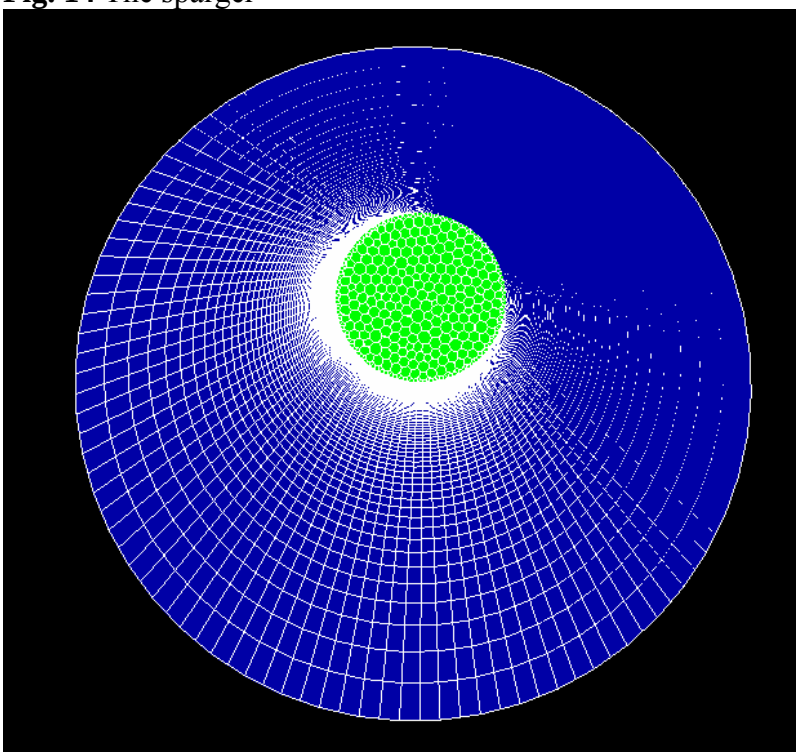

Fig. 15. Top view of fluidized bed column

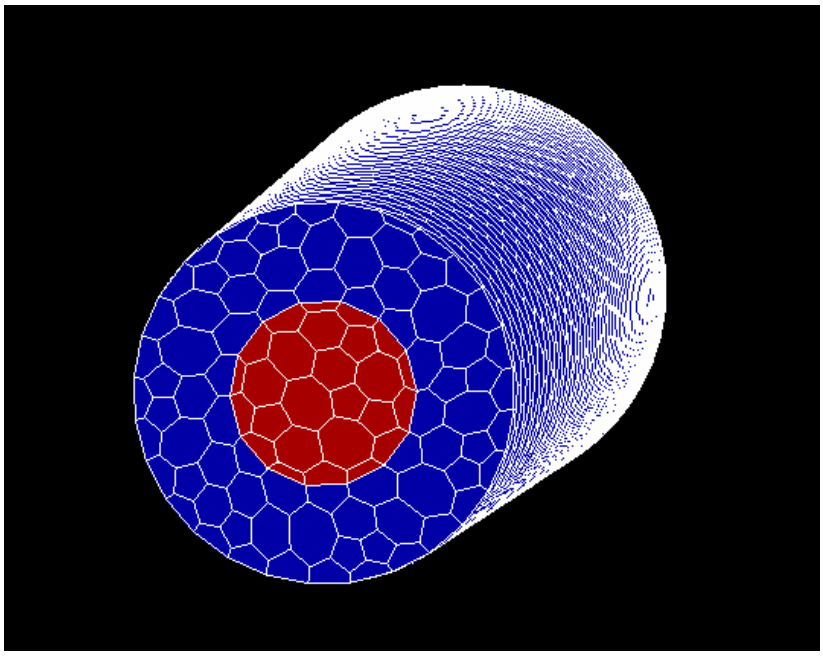

Fig. 16. Isometric view of bottom distributor section

Firstly the fluidized bed is solved for only water phase. The default solver is used for analysis. The multiphase analysis disabled and energy calculation off as we are not considering heat transfer. Realizable K-epsilon model is used for viscous analysis. Standard wall functions are used for the analysis. Water material is selected from the fluent database and used as liquid phase.

As only single phase analysis is being done with water as a liquid phase air inlet, which is through sparger, is defined as a wall. The model is initialized with only water as a velocity inlet. The turbulence intensity is kept at 0.5 and turbulence viscosity ration is 10. The convergence criteria is set at 0.0001 for all equations. The model is solved for steady state analysis. The solution is converged at 130 iteration. Velocity profile, volume fractions and velocity vectors were checked and found to be as required.

Now the fluidized bed is solved for two phase namely water and gas. The multiphase analysis is enabled. Air material is added from the fluent database. Water is set as primary phase and air as secondary phase. . Realizable K-epsilon model is used for viscous analysis. Standard wall functions are used for the analysis. Air material is selected from the fluent database and used as gas phase. The Gidaspow model is used for the gas-liquid phase interaction. As Gidaspow model is based on multi scale resolution of system will gives best results as it is best suited for complex three phase fluidization system. Boundary conditions are given for the liquid and gas phase. Velocity of each phase is given. The volume fraction of air is set to1 for air inlet at the sparger. The fluidized bed system is solved for steady state analysis. The results are obtained and reviewed. The velocity vectors for gas phase are shown below

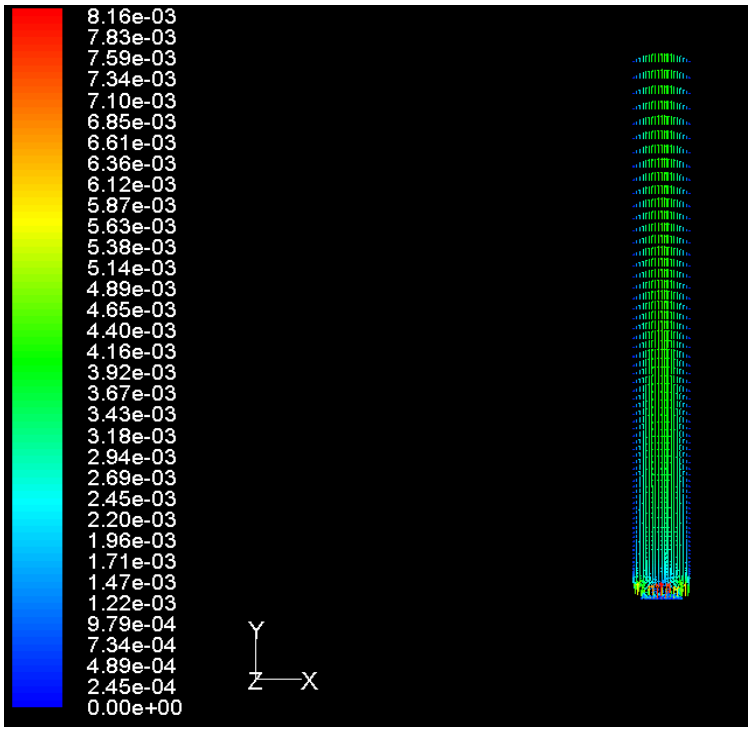

Fig 17. Velocity vectors of air for air – water two phase simulation

Now the fluidized bed is solved for three phases. Air, water and glass beads are used as gas phase, liquid phase and solid phase respectively. The analysis is enabled for three phases. Water is set as primary phase and air and beads are selected as secondary phases. Beads are selected as new material. Its properties are set like diameter and density etc.

Now boundary conditions are set for three phase fluidized bed. The air, water are set as velocity inlet and outlet as pressure outlet. The gas and liquid superficial velocities are set. The Gidaspow model is selected for the gas-liquid, liquid-solid and gas-solid interactions. The solid volume fraction is pached in the bottom test section. To get the actual idea how fluidized bed behaves with time the model is solved for transient analysis with time step 0.01s and 15 maximum iterations per time step. The model is solved for 10 seconds. The results are obtained for volume fraction of each phase, velocity vectors of each phase and velocity profile of each phase. The gas and liquid superficial velocities are varied over a broad range of operating conditions. Results are obtained for each solves and compared with the actual results got in the experimental work reported in the literature.

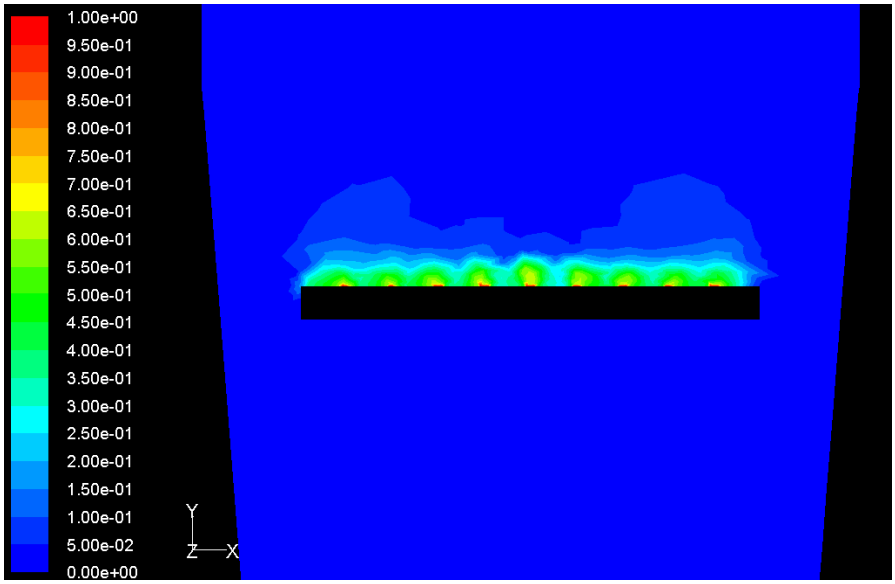

Fig. 18) Formation of gas bubbles at the sparger

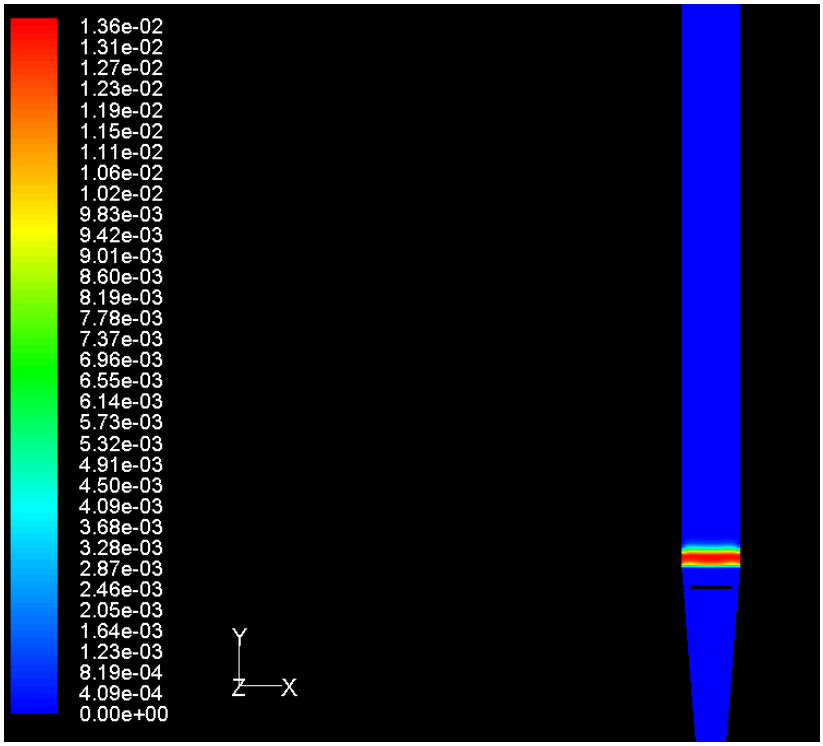

Fig. 19) Solid holdup at time 1.5 sec at Ul = 0.04 and Ug = 0.02,
dp = 2.5mm, ρ_p = 1700 kg/m^3

The non-uniform expansion of solid particles is due to the fact that the water rising from the inlet hits the sparger and passes through the annulus space created between the sparger and cylinder. This creates wakes at the top of sparger.

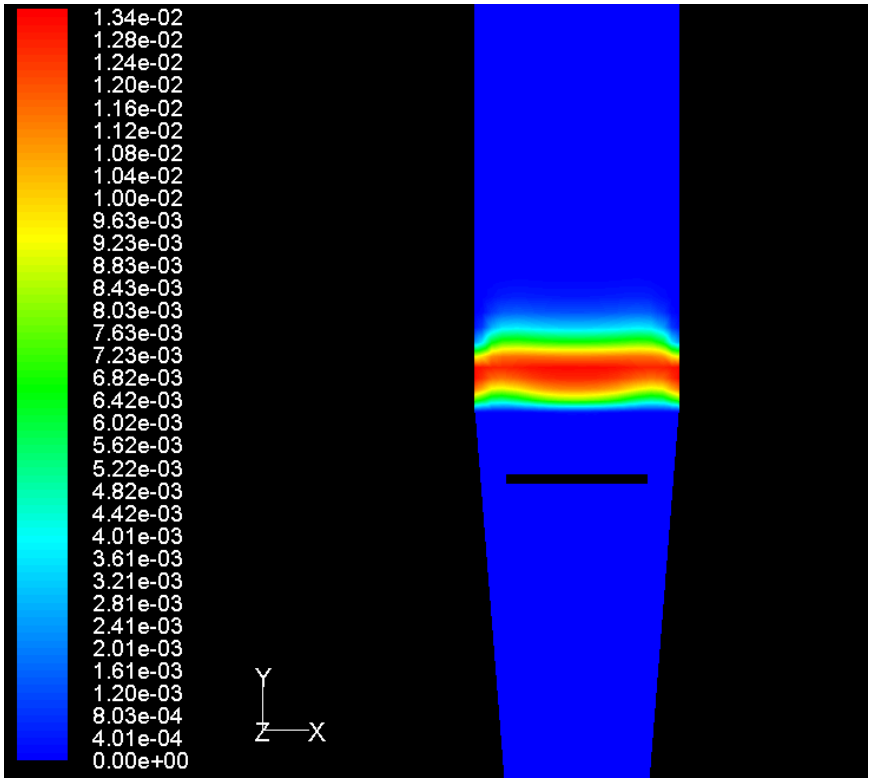

Fig. 20. Solid holdup at time 2.8 sec , Ul = 0.04 and Ug = 0.01, dp = 2.5mm, ρ_p = 1700 kg/m^3

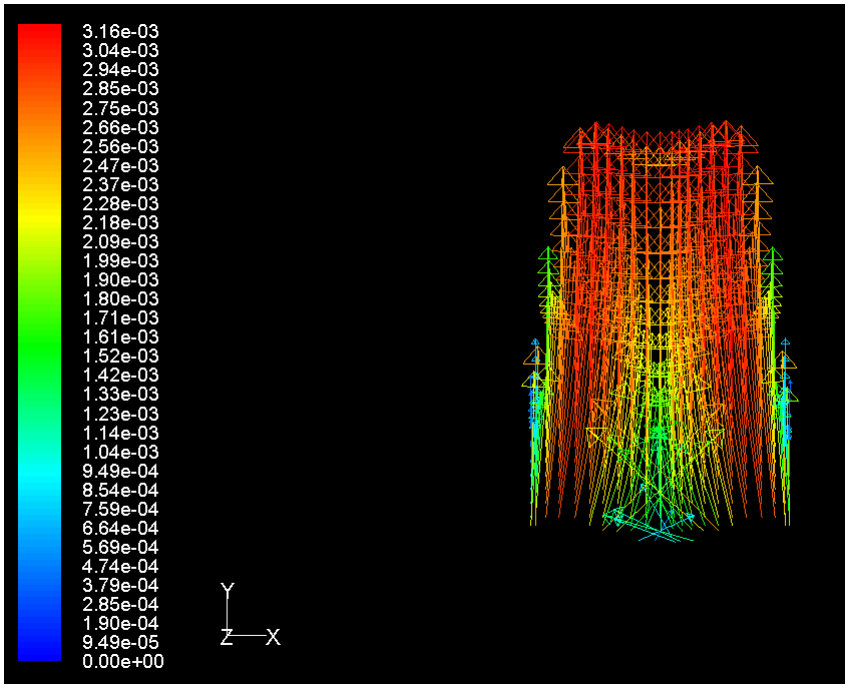

Fig. 21. Solid particles velocity vector at 3 sec., Ul = 0.04 and Ug = 0.01 at Ul = 0.04 and Ug = 0.01, dp = 2.5mm, ρ_p = 1700 kg/m^3

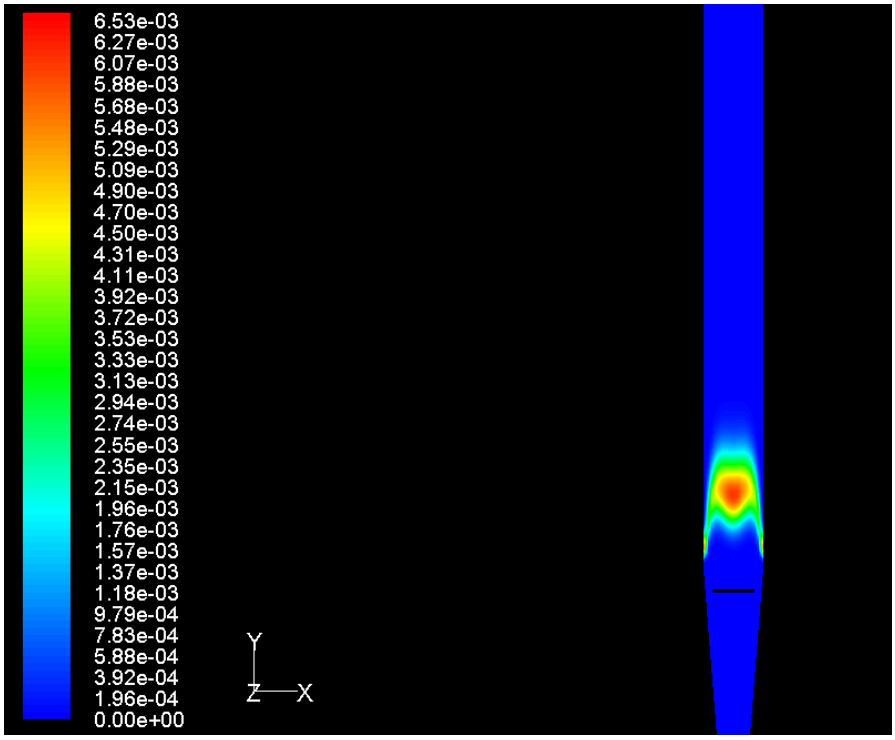

Fig. 22) Solid holdup at 4.2 sec ,Ul = 0.04 and Ug = 0.01,
dp = 2.5mm, ρ_p = 1700 kg/m^3

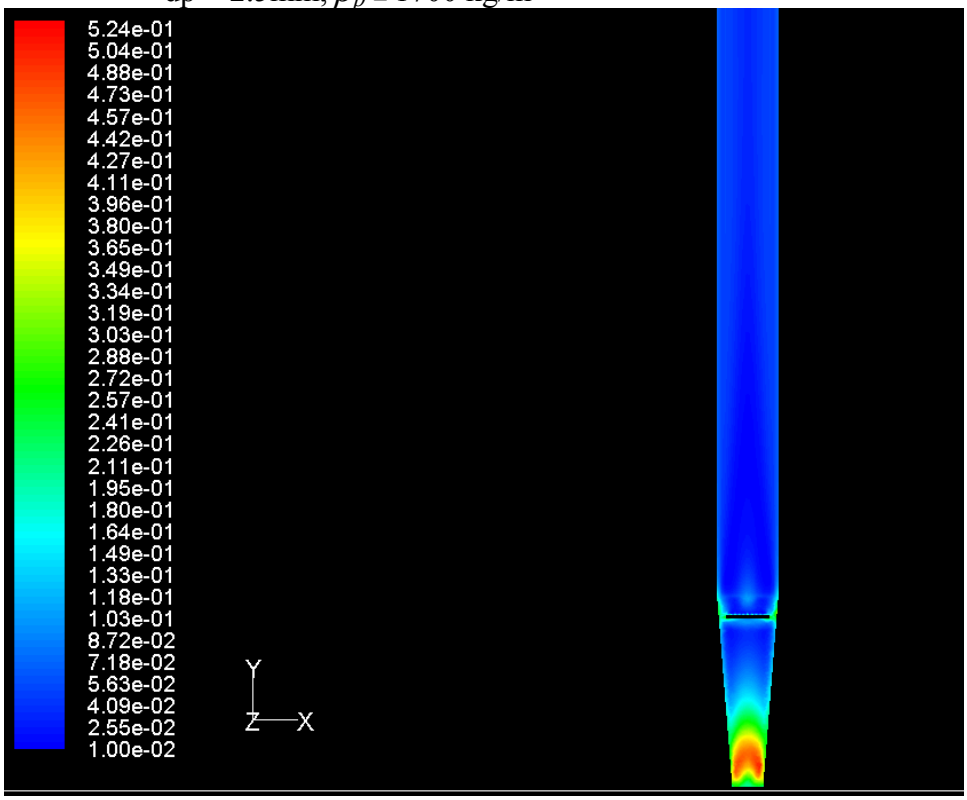

Fig. 23) Turbulent intensity at 4.2sec. ,Ul = 0.04 and Ug = 0.01,
dp = 2.5mm, ρ_p = 1700 kg/m^3

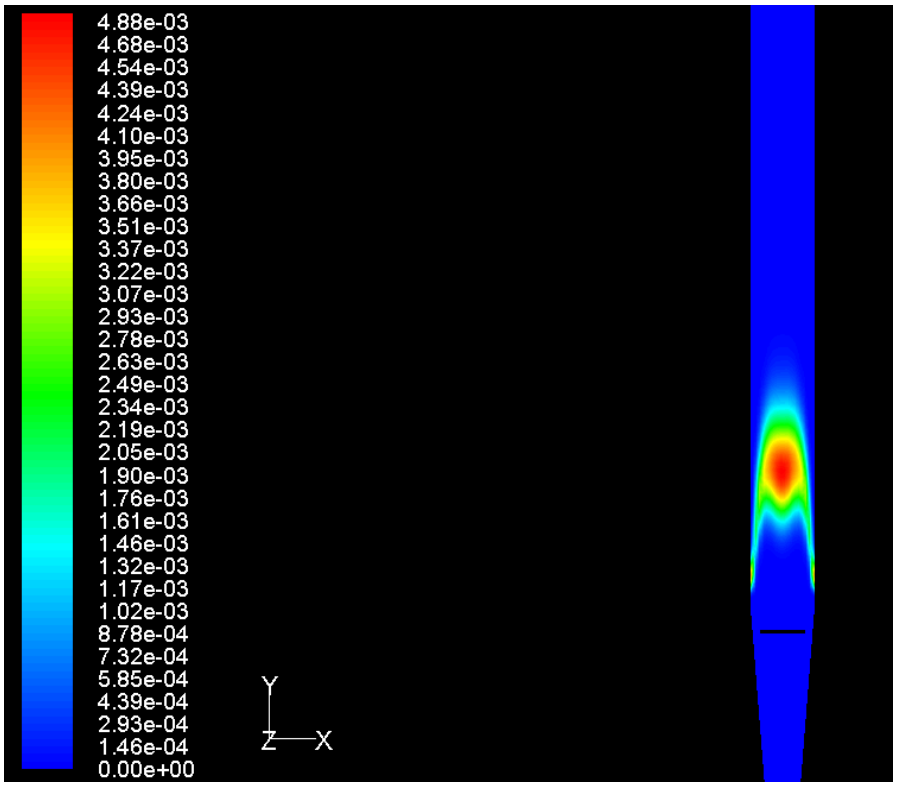

Fig. 24) Volume fraction of glass beads at 5.9 sec Ul = 0.04 and Ug = 0.01, dp = 2.5mm, ρ_p = 1700 kg/m^3

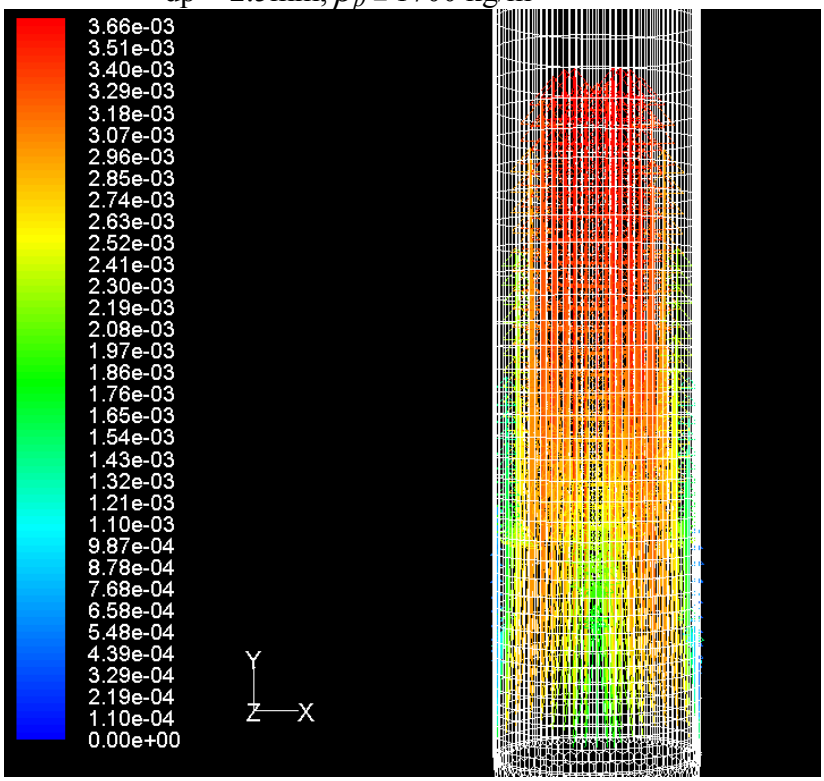

Fig. 25) Velocity vectors of glass beads at 6.3 sec

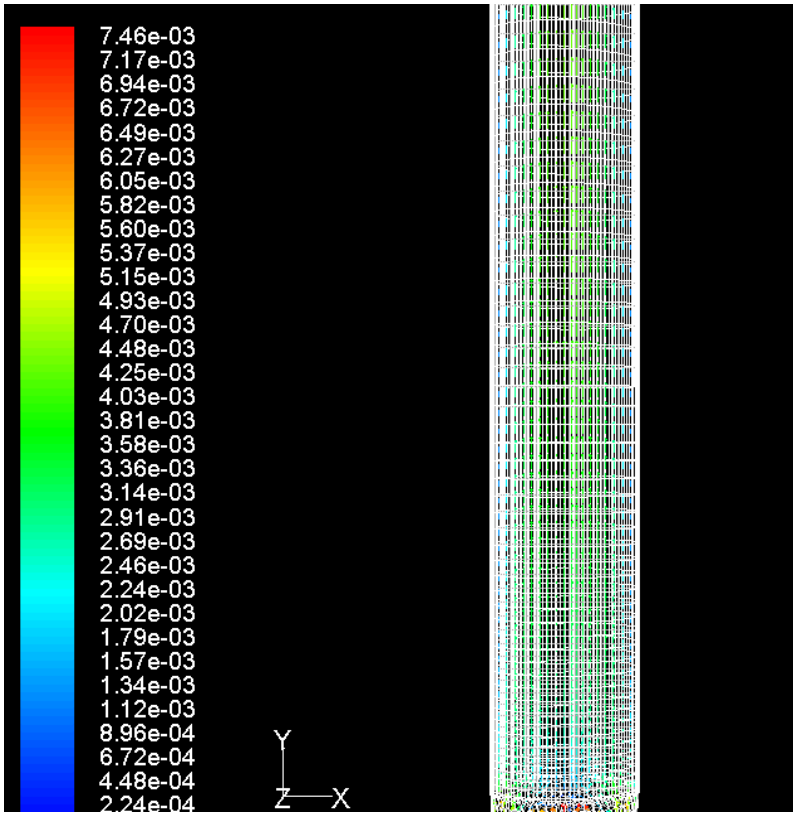

Fig. 26) Velocity magnitude of air at 6.8 sec

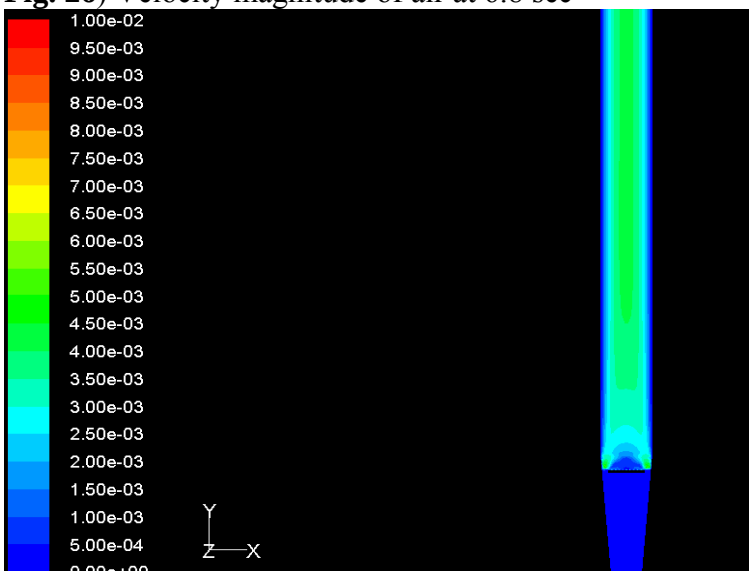

Fig. 27) Velocity profile of air at 7.2 sec.

The above figure shows that there is rise in the bubble rise velocity where particles are located. The velocity vectors of air shows that there is considerable redistribution bubbles takes place only when they comes into contact with the liquid-solid suspension containg high concentration of solids.

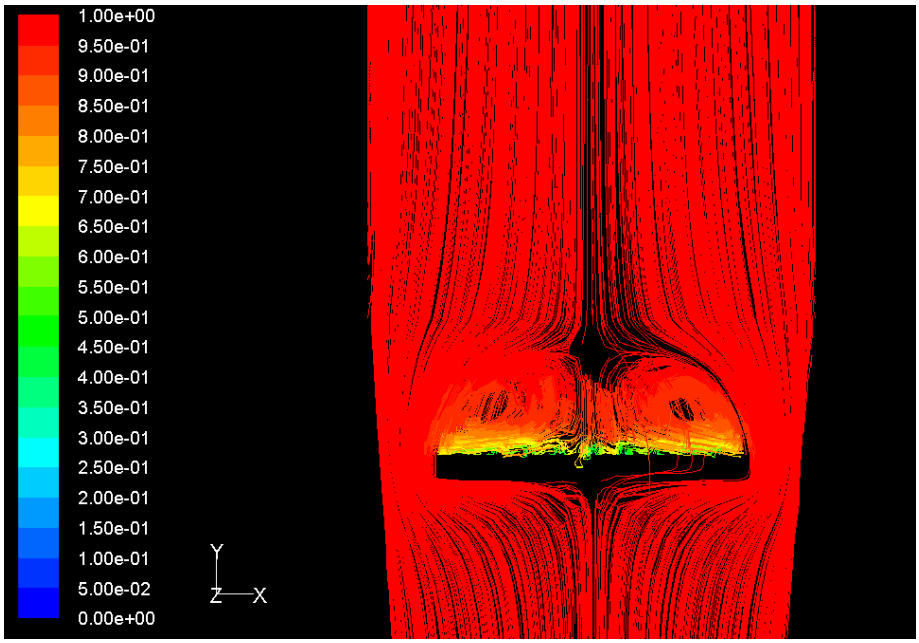

Fig. 28) Path lies for fluids in three phase fluidized bed.

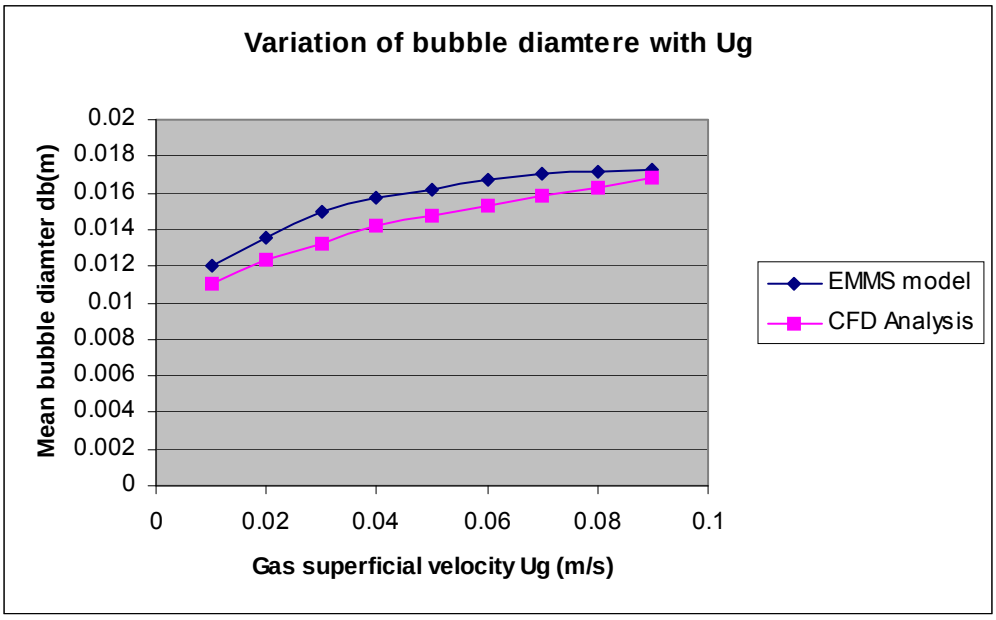

Fig. 29) Variation of mean bubble diameter with gas superficial velocity.
Ul= 0.04 m/s dp = 2.5mm

The above figure shows that the mean bubble rise velocity increases with increase in gas superficial velocity. The increased gas velocity induces bubble coalescence, which tends to increase the bubble diameter. The EMMS model over predicts the bubble diameter as the particle-particle collision, wall effects are not considered.

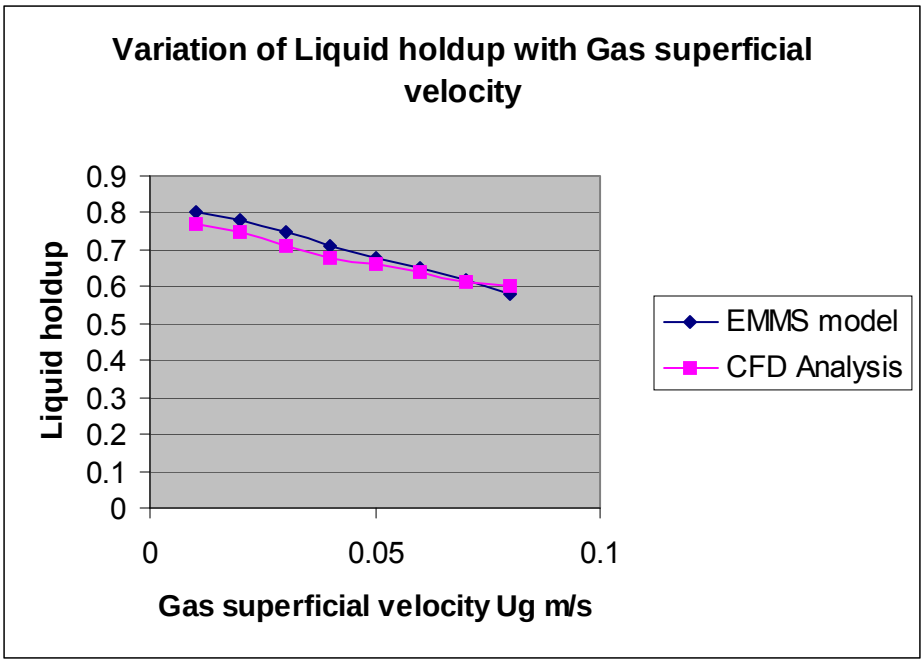

Fig. 30) Variation of liquid holdup with gas superficial velocity at Ul = 0.04m/s

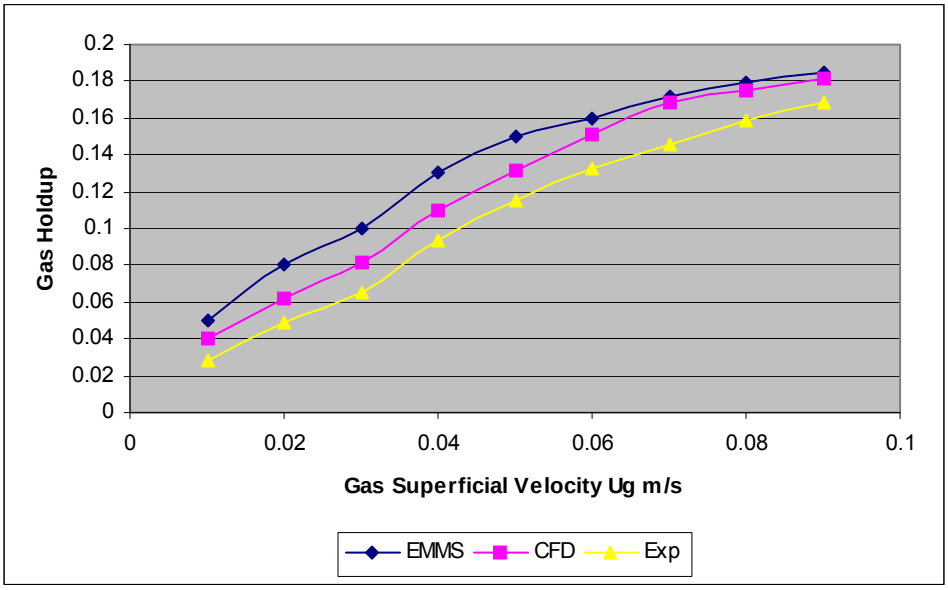

Fig. 31) Variation of gas holdup with gas superficial velocity. Ul = 0.04,

The Fig. 30 and Fig. 31 indicated that the gas holdup is strong function of gas superficial velocity. The increase in gas velocity increases the gas holdup and decreases the liquid holdup.

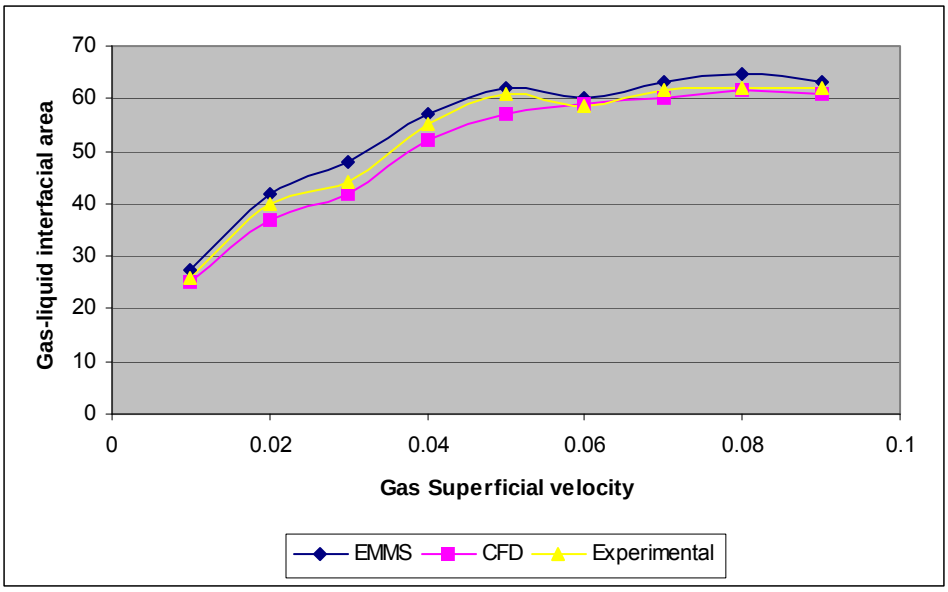

Fig. 32) Variation of gas-liquid interfacial area with gas superficial velocity Ul = 0.04 m/s, dp = 2.5mm

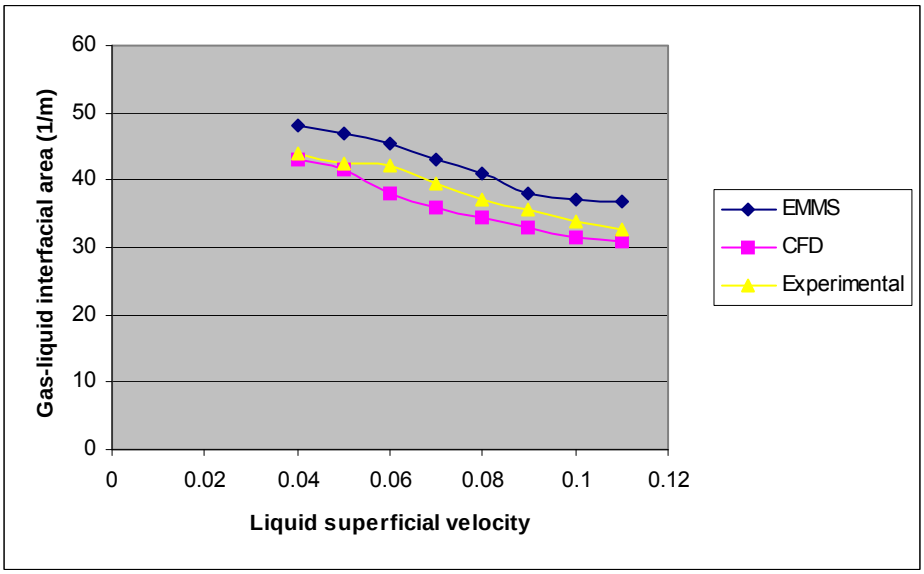

Fig. 33) Variation of gas-liquid interfacial area with liquid superficial velocity Ug = 0.02 m/s,

The above figures shows that the gas-liquid interfacial area is inverse finction of liquid superficial velocity. The increase in liquid superficial velocity causes increase in liquid holdup and subsequently decreases the gas holdup. The interfacila area increases with increase in gas superfcial velocity. From the figure it can be seen that firstly the increase in gas velocity causes increase in interfacial area but further increase causes the bubble coalscence which tends to increase the bubble diamter hence actually decreaseing the gas-liquid interfacial area.

6.0 Gas-liquid interfacial area in three phase semi-fluidized bed

Semi-fluidized bed is considered as series combination of bottom fluidized bed and top packed bed and study on gas-liquid interfacial area is done accordingly. . The gas liquid interfacial area for semi-fluidized bed is calculated by using weighted average of interfacial area for top packed bed and interfacial area of bottom fluidized bed

The EMMS model developed for fluidized bed is used for the calculation of gas-liquid interfacial area in the bottom fluidized bed. The height of top packed bed and bottom-fluidized bed is known form the experiments done and hence used in the calculations. For the top packed bed the gas–liquid interfacial area is calculated by using the approach followed by Faical Larachi and co researchers. The procedure followed in the calculation if interfacial area for top packed bed is explained below.

6.1 Modeling:

Gas-liquid interfacial areas in top packed bed is closely related to bubble sizes.In gas-liquid emulsions under turbulent flow, bubble sizes are probably determined by the dynamic pressure forces caused by changes in velocity over distances at most equal to the bubble diameter .Hence, as postulated by Lara Marquez et al [5], bubble diameter would be proportional to the microscale of turbulence given by the Kolmogoroff relation between the turbulance scale and the power dissipation rate $\xi_{LG.}$

However, for highly viscous liquids and moderate gas velocities bubble size is probably imposed by a competition between the viscous shear of the gas-liquid emulsion that tends to deform and break the bubble, and the force induced by interfacial tension that tends to stabilize the bubble.

The maximum stable bubble diameter in a liquid emulsion may be obtained from the following expression :

$$\Omega_c = \tau D_{max} / \sigma_L \qquad (23)$$

where τ is the external force acting on the bubbles, which tends to deform and break them; D_{max} is the maximum bubble size that can stand the external force without being broken, and σ_L the interfacial tension. Hence,Ω_c is a critical dimensionless, number that gives the conditions at bubble burst resulting from the competition between the external force given by D_{max}/σ_L .

As mentioned above, for turbulent flow, dynamic pressure forces of the turbulent motions are responsible for bubbles deforming and break-up. Taking into account the Kolmogroff relation between the turbulence scale and the power dissipation rate ξ_{LG}, the external force acting on the bubbles may be expressed by:

$$\tau = \Gamma \sigma_L (\zeta_{LG} D_{max} / \rho_L)^{2/3}$$

where Γ is the external constant.

A constant ratio between the Sauter diameter and the maximum bubble diameter, $D_{3,2} \cong \alpha D_{max}$, may be assumed. Furthermore, D, is related to the gas-liquid interfacial area and the liquid hold-up according to:

$$D_{3,2} = \alpha D_{max} = 6 (1 - f_L) / \Lambda \qquad (24)$$

Hence considering Eqs.(1)-(3) after rearrangements, the expression for a correlation for estimating gas-liquid interfacial areas given in [1] is obtained:

$$\Lambda / \Lambda_0 = \kappa (1 - f_L) d_h (\rho_L / \sigma_L^3)^{0.2} (\zeta_{LG})^{0.4} \quad (25)$$

Where κ is the parameter fitted from experimental data.

When semi-fluidized beds are operated with highly viscous liquids and moderate gas velocities, bubble sizes in the top packed bed may be determined by the gas-liquid emulsion viscous shear. For this simulation, Taylor's theory [5] has been taken into account together with subsequent investigations on bubble deformation and break-up in sheared emulsions. In this case, the dimensionless number that gives the force ratio Ω_c is usually called the capillarity number. Since the ratio of dispersed to continuous phase viscosities.λ, considerably affects the bubbles stability. Bently and Leal have suggested a theory for large bubble deformations for estimating Ω_c. The theory is valid for gas-liquid viscosity ratios lower than 0.02, where the critical capillarity numbers are large and depend upon the viscosity ratio. According to this theory, Eq.(23) becomes:

$$\Omega_c = \tau D_{max} / \sigma_L = C_1 \lambda^{-1/6} \quad (26)$$

In this case, the external force acting on the bubbles τ, arises from the viscous stress exerted by the gas-liquid emulsion. This force can be evaluated as the product of the effective emulsion viscosity and the maximum liquid velocity gradient. Bubbles in sheared emulsions generally break into ones of similar sizes and produce some bubbles depends on the way the liquid gradient is established. If the rate of increase in liquid gradient until the one that produces the break is small, only a few satellite bubbles are produced [5]. Moreover, for low viscosity ratios ($\lambda <= 0.02$), bubbles are deformed as spheroids with pointed ends from which only small micro bubbles are ejected, known as the tip spinning mechanism[5].

The following assumptions have been made to get a mean bubble diameter, hence the gas-liquid interfacial area representative for the gas-liquid mass transfer phenomenon:

- Very small satellite bubbles formed in the break-up do not significantly contribute to gas hold-up and gas-liquid mass transfer. Therefore, only relatively large bubbles (between 0.1 and 1 mm) are considered.
- Effective viscosity of the gas-liquid emulsion is estimated according to Einstin's equation [14] taking the coefficient 2.5, which is strictly valid for simulations of rigid spheres,for the sake of simplicity:

  $$\mu_L^* = \mu L(1 + 2.5 (1 - f_L)) \quad (27).$$

- The liquid velocity gradient is supposed to be the ratio of the interstitial liquid velocity and a mean porous radius, calculated considering the fixed bed as a set of tortuous cylindrical tubes:

  $$r_p = 2 \varepsilon / \Lambda_c \quad (28)$$

Replacing τ and D_{max} in Eq.(26) and using Eqs (27) and (28), the following relation arises:

$$6g(1 - f_L)/ \Lambda = (\alpha C_1 \sigma_L / \mu^*_L)(\varepsilon f_L 2\varepsilon / u_L \Lambda_c) \lambda^{-1/6} \quad (29)$$

Eq. (29) constitutes a one parameter correlation for estimating 'Λ' in FBR with highly viscous liquids.To establish conditions for which it can be used, the criterion that viscous shear force are larger than dynamic pressure forces of the turbulent motions is employed. Following the work of Hintze , the last condition may be expressed as:

$$\mu^*_L(u_L/\varepsilon f_L \bar{r}_p) > \Gamma\rho_L((\xi_{LG}/\rho_L)D_{max})^{2/3} \quad (30)$$

Where Γ may be taken as 2 according to Batchelor and (ξ_{LG}/ρ_L) is the two-phase flow dissipation power rate per unit mass. Approximating D_{max} to the particle diameter, rearranging and asking that the viscous shear would be 10 times larger than the inertial forces, the criterion becomes :

$$\mu^*_L > 10[(\xi_{LG}d_p)^2\rho_L]^{1/3}\varepsilon f_L d_h/u_L \quad (31)$$

It has been found that pressure has a strong effect on gas-liquid interfacial areas in the top packed bed [5]. For very low liquid or gas flow rate .an increase in *a* for gas superficial velocities above a critical value. The higher is the liquid flow rate, the larger is the pressure influence .Gas and liquid superficial velocities over which pressure effects are no longer negligible coincide with the ones over which gas hold-up starts to exhibit pressure dependence. Hence, a relation between the change in interfacial areas and hold-ups due to pressure is expected. For velocities higher than these critical values, an increase of either the gas or the liquid flow rate induces a increase in *a*.

A physical hypothesis that explains the experimental observations has already been suggested in a previous publication. As pressure or gas density increases, gas shear over the liquid film becomes more important for the same superficial gas velocity. The momentum transfer through the gas-liquid interface may then be large enough so as to cause gas to be entrained into the liquid, especially at certain points where the particles leave very small interstitial space. The gas will disperse in the liquid film forming bubbles. The bubbles formed will then be transported in the liquid films with no slip velocity, increasing gas hold-up and also the interfacial area between the fluids.

To evaluate a mean bubble diameter, similar assumptions as for the case of sheared emulsions have been postulated taking into account that the liquid velocity in the trickling flow regime is generally very slow; hence, viscous forces are likely to predominate. In this case, bubbles Sauter diameter can be defined by:

$$D_s=6 f_L^b \varepsilon/\Lambda_b=6(f_L^b-\beta_L)\varepsilon/(\Lambda-\Lambda^o) \quad (31)$$

where f_L^b and Λ_b are, respectively, the excess gas hold-up (expressed as a percentage of the bed porosity) and the gas-liquid interfacial area induced by the presence of bubbles in the liquid films. Such bubbles do not exist at atmospheric conditions in the trickle flow regime. At elevated pressures they may be evaluated from the difference between the actual values of gas hold-up and interfacial area and those corresponding to atmospheric conditions, as exposed in Eq. (31). To get Eq. (31), a negligible effect of pressure on the wetting efficiency has been considered. The effective emulsion viscosity is also expressed in terms of f_L^b as follows:

$\mu^*_L=\mu_L(1+2.5(f_{Lb}/(f_{Lb}+f_L))= \mu_L[1+2.5(1-f_L/f_L^o)]$ (32)

From Eq. (31) and Eq. (24) with a convenient numerical constant, and writing the liquid velocity gradient as the retio of the interstitial liquid velocity and the liquid film thickness δ_L, the following expression is obtained:

$6(f_L^o - f_L)\varepsilon/(\Lambda - \Lambda^o)=\alpha C2(\sigma L\delta L\varepsilon f_L/\mu_L^* \mu_L)\lambda^{-1/6}$ (33)

Taking $\kappa_2=(6/\alpha C_2)$, replacing the effective viscosity and rearranging, Eq. (33) becomes:

$\Lambda = \Lambda^o+\kappa((f_L / f_L^o)-1)[1+2.5(1-f_L / f_L^o)](We_L/Re_L)(\lambda^{1/6}/ \delta_L)$ (33a)

Here We_L and Re_L and the physico-chemical properties of the liquid phase.

To evaluate the film thickness δ_L, two approaches have been followed:

- First,and for the sake of simplicity, δ_L was assumed to remain unchanged under high pressure conditions.Hence, it can be approximated by the ratio of liquid hold-up and gas-liquid interfacial area at atmospheric pressure, $\delta_L=(\varepsilon \beta_L^o/ a^o)$.
- The second approach was to formulate and solve a momentum balance assuming:
  I) Unidirectional and vertical liquid flow
  II) Negligible amount of dispersed gas in comparison with the continuous gas
  III) frictionless gas plug flow for the continuous gas
  IV) gas-liquid slip ratio estimated

Results obtained with both procedures were not significantly different in terms of uncertainties in interfacial area productins. Therefore, the simpler way is recommended and results obtained by this procedure are shown hereafter. Replacing δ_L in Eq. (33a), it arises:

$\Lambda = \Lambda^o\{1+\lambda^{1/6}\kappa_2 (We_L/Re_L)[1+2.5(1-f_L / f_L^o)](1/f_L -1/f_L^o)\}$ (34)

The gas-liquid interfacial area is evaluated from the top equation.

6.2. Model solution and validation:

The above set of equations is solved for wide range of gas and liquid superficial velocity. The gas and liquid holdup is obtained from the CFD analysis of the three phase semi-fluidized bed done. Results were obtained for each of the top packed bed and bottom fluidized bed. The weighted average is done on the basis of solid particle mass in each of the section. As there is no experimental data available in the literature the individual results of fluidized bed and packed bed were compared with that of fluidized bed and packed bed.

7 CFD Analysis of three phase semi-fluidized bed for gas-liquid interfacial area.

Procedure followed for analysis of three phase-fluidized bed is used in the analysis of three of three phase semi-fluidized bed. Geometry of the actual semi-fluidized bed is created in the GAMBIT. The whole semi-fluidized bed column is divided into four sections namely the bottom distributor section, the bottom test section where solids particles are placed initially, the fluidization zone and the section above the top perforated grid. The semi- fluidized bed column is meshed as in case of fluidized bed.

The fluidized bed is meshed and file is exported to Fluent. The meshed grid is shown in figure below.

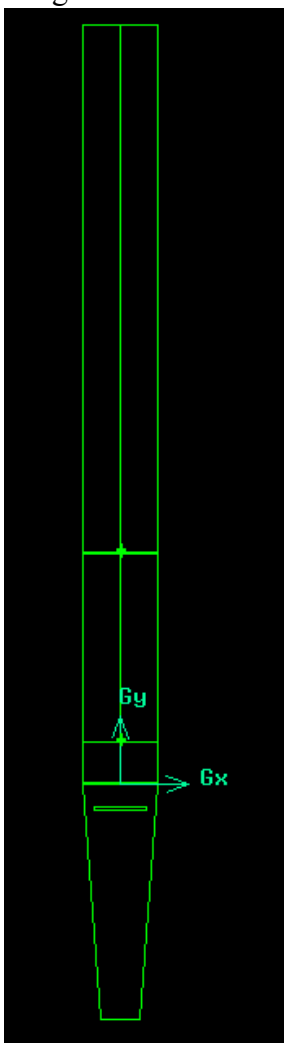

a)

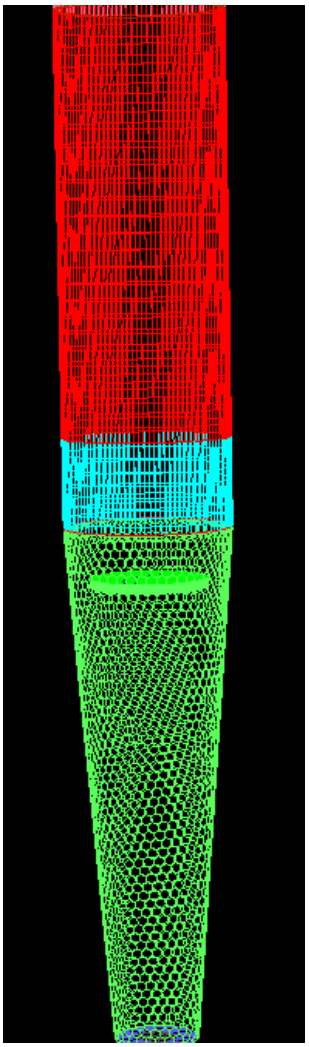

b)

Fig 33a) Geometry of semi-fluidized bed.
Fig. 33b) Meshed semi-fluidized column

The semi-fluidized bed is solved initially for water phase only. The steps followed in fluidized bed are adopted over here also. Results were obtained and reviewed. Now the semi-fluidized bed is solved for gas and liquid phase. Liquid phase is set as primary phase and gas phase as secondary phase. Boundary conditions are set and velocity magnitude is set for both the gas and liquid phase. Model is solved for steady state iteration with convergence criteria equal to 0.001 for all equations. Solution is obtained and results were tested.

Now the semi-fluidized bed is solved for three phase analysis. Water, air and glass beads were selected as liquid phase, gas phase and solid phase respectively. The semi-fluidized bed is solved by using Eulerian model, Boundry conditions were set. For multi phase interaction Gidaspow model is used. Realizable K Epsilon model is used for turbulent stress modeling. The velocity magnitude were given for each phase inlet. the bottom test section is patched with the solid particles with its volume fraction. The semi-fluidized bed is solved for transient analysis with time step 0.01 sec and maximum iterations per time step set to 15. Results were reported at each 25 iterations.

After the solution is converged the results were obtained and compared with the experimental results in the literature. The results obtained at various time steps are reported below.

7.1 Results of CFD and EMMS analysis:

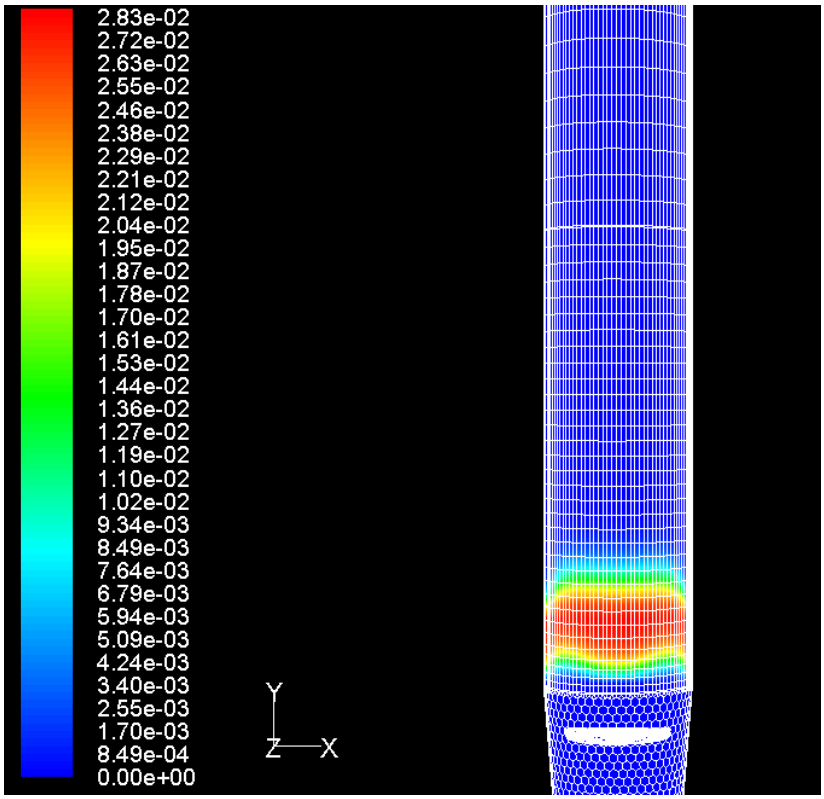

Fig. 34) Solid particle holdup at 2sec with Ug = 0.03, Ul = .05

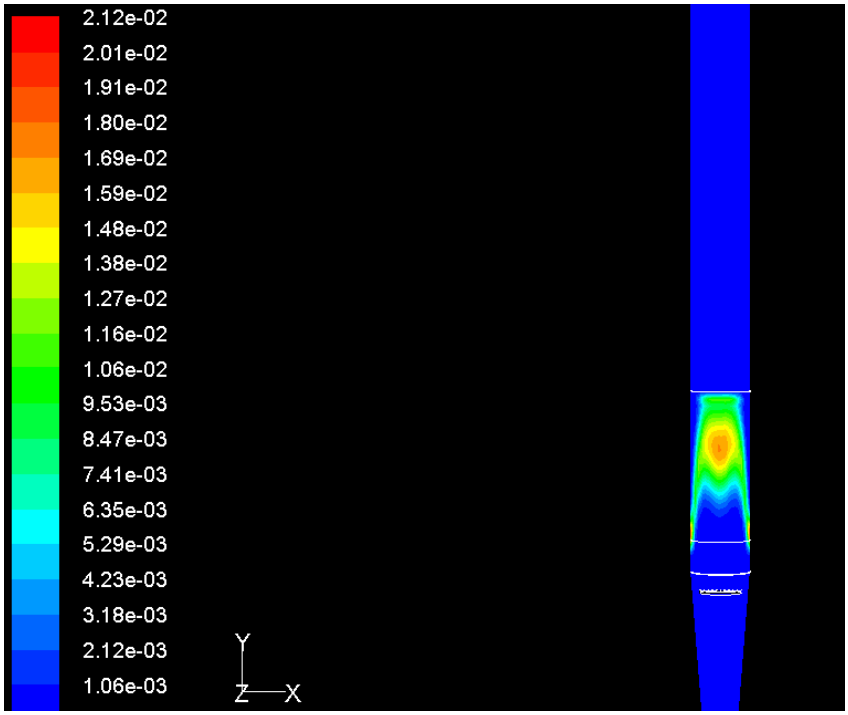

Fig. 34) Solid particle holdup at 5sec with Ug = 0.03, Ul = .05

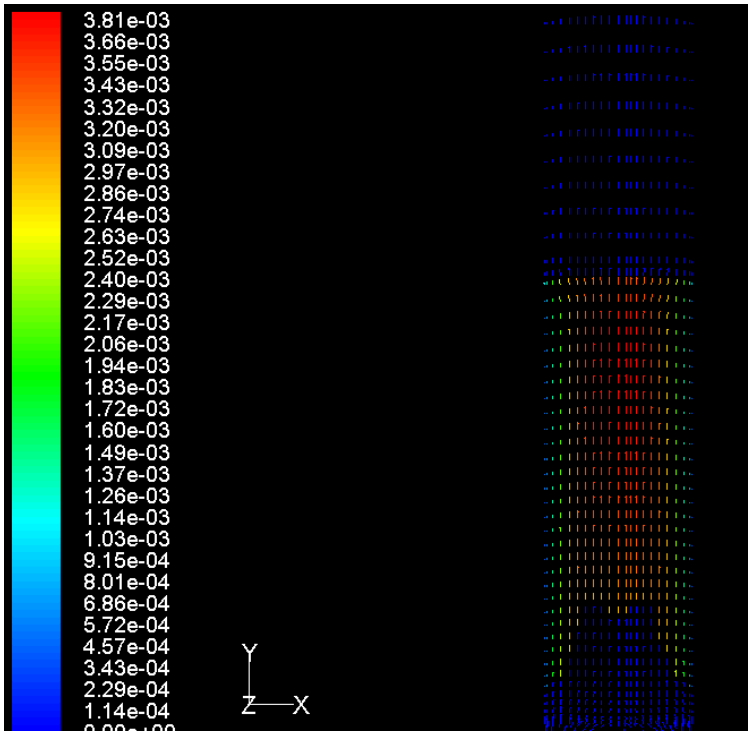

Fig. 35) Solid particle relative velocity vector with air with at 5sec with Ug = 0.03, Ul = .05, dp = 2.5mm

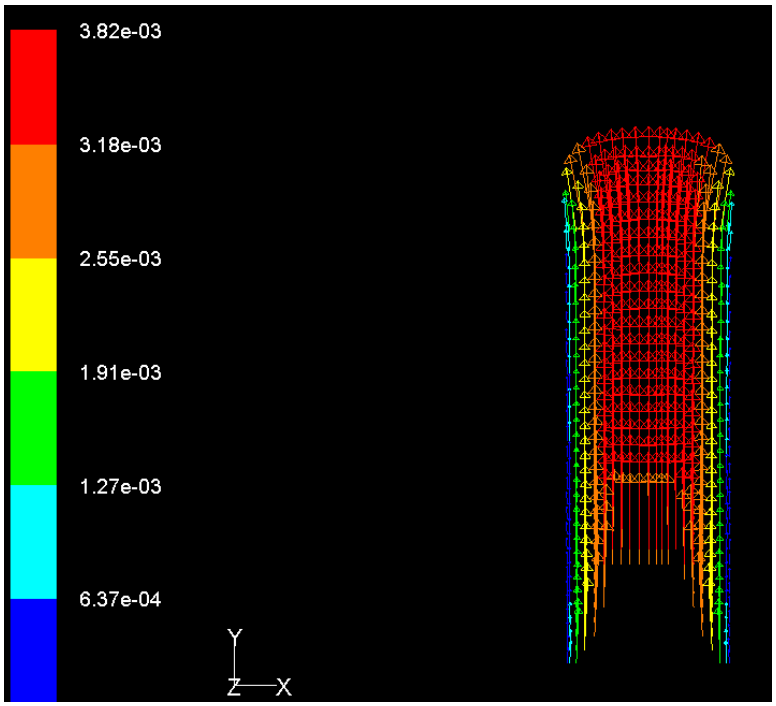

Fig. 36) Velocity vector of solid particles at time 5 sec

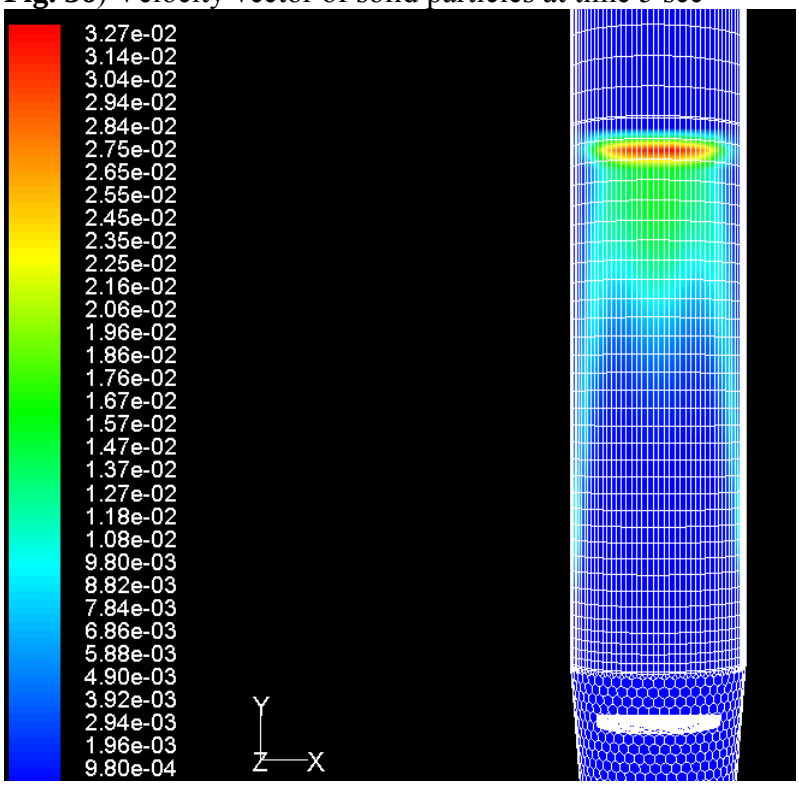

Fig. 37) Solid particle holdup at 7sec with Ug = 0.03, Ul = .05

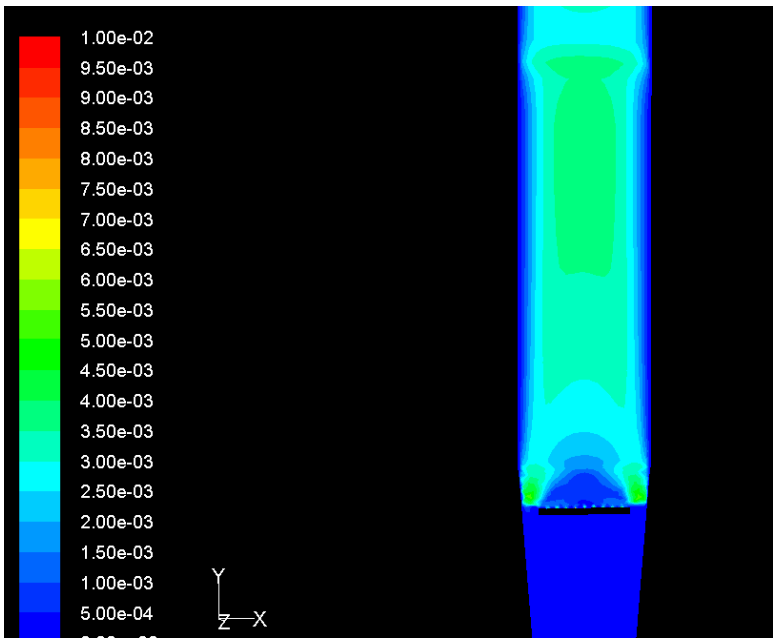

Fig. 38) Velocity profile of air at 7 sec with Ug = 0.03, Ul = .05

The above figures show that there is maximum particle flow at the center of the column. The gas phase flow is also maximum at the center of the column. The gas phase redistribution can be clearly seen form the figures. The redistribution of gas bubbled into smaller ones, which can pass through the small capillaries of the packed bed decreases the mean bubble diameter hence increasing the gas-liquid superficial velocity.

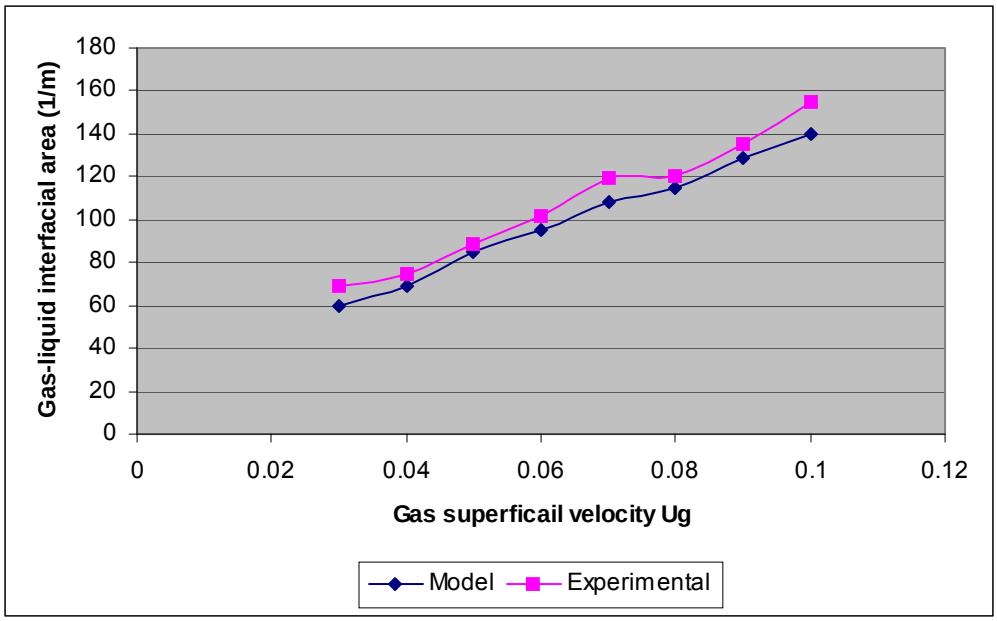

Fig. 39) Variation of gas-liquid interfacial area with gas superficial velocity. At Ul = 0.06m/s

The above figure shows that the gas-liquid interfacial area increases with increase in gas superficial velocity. The increase in interfacial area is due to two reasons. the gas holdup increases with increase in gas velocity. As the gas velocity is increased the height of the top packed bed also increases. The increase in the height of the top packed bed causes the gas redistribution at very early stage of passage and hence reduces the bubble coalescence, which increases the gas-liquid interfacial area.

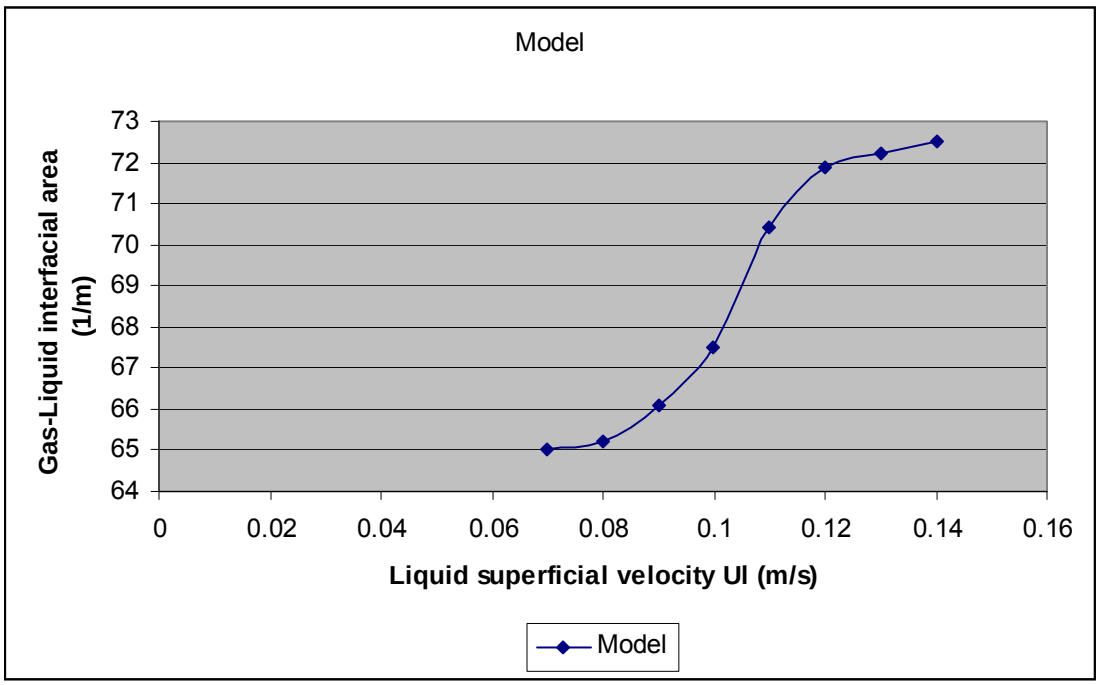

Fig. 40) Variation of gas-liquid interfacial area with liquid superficial velocity at Ug= 0.03m/s and dp = 2.5mm and ρ_p = 1800 kg/m^3

The above figure shows the distinct behavior of the three phase semi-fluidized bed. With increase in liquid velocity the gas phase holdup decreases. The effect of decrease in gas holdup is eliminated by the fact the there is increase in the height of the top packed bed. The increase in packed bed height causes bubbles to split at very early stage. The smaller is the bubble diameter larger is the gas-liquid interfacial area. The increase in interfacial area is observed up till the whole semi-fluidized bed is converted into packed bed. After the semi-fluidized bed is fully converted into the top packed bed the interfacial area remains constant.

8 Conclusion

The EMMS model is solved for three phase-fluidized bed. The effects of bubble wakes are considered in the analysis. The gas liquid interfacial area for fluidized bed is evaluated bu using the EMMS model. The CFD analysis of the three phase fluidized bed is also done. The reulst from EMMS model and CFD analysis are compared with the experimental results reported in the literature. The EMMS model slightly over predicts the phase holdup as compared to the results from CFD analysis

The difference in the results of EMMS model and experimental may be due to the fact that the particle-particle collision and wall effects are not considered in EMMS model. The CFD analysis is successfully done and behavior of the fluidized bed over a time period is observed. The results from EMMS model and CFD analysis are found satisfactory and below 24 percent error.

It is found that the gas-liquid interfacial area increases with increase in gas velocity but decreases with increase in liquid superficial velocity.

The gas-liquid interfacial area for Semi-fluidized bed is evaluated by weighted average method. The results were obtained and compared with experimental results for each fluidized and packed bed.

It is found that the increase in gas velocity in semi-fluidized bed increases the gas-liquid interfacial area much larger than in fluidized bed. The redistribution of gas phase into smaller bubbles helps in increase in interfacial area.

Nomenclature

b	width of the bubble (horizontal or major axis of the bubble
$d_{3,2}$	Sauter mean bubble diameter determined by the maximum bubble theory (m)
d_b	mean bubble diameter (m)
Eo	Evotvos number, $Eo = g(\rho m - \rho g)d2$
f_g	gas holdup
f_w	bubble wake holdup
k_0	mean relative size of the wake behind a single bubble (Vw/Vb)
Mo	Morton number,
N_d	power dissipated in particle collision, circulation, acceleration, liquid viscous dissipation with respect to unit mass of particles (J/(s kg))
Nsur	power consumed for increase of bubble surface energy with Respect to unit mass of particles (J/(s kg))
Nst	power consumed for suspending and transporting unit mass of particles (J/(s kg))
NT	total power consumed with respect to unit mass of particles (J/(s g))
Reb	gas Reynolds number with the characteristic length of bubble width,
Red	gas Reynolds number with the characteristic length of mean bubble diameter.
Re□g	modified gas Reynolds number, Re□g = RelUg/Ul
Re_l	particle Reynolds number, Rel = ρldpUl/μ−1
u_b	bubble rising velocity (m/s)
ub,i1	gas superficial velocity in inter-phase 1, ub,i1 = ubfg/(1-fw)

u_{dc}	particle superficial velocity in the liquid–solid mixture (m/s)
$u_{m,i1}$	liquid–solid suspension superficial velocity in inter-phase 1
$u_{m,i2}$	liquid–solid suspension superficial velocity in inter-phase 2
$u_{w,i2}$	bubble wake superficial velocity in inter-phase 2, ub,i1 = *u*b*f*w/(1−*f*g)
ut	terminal velocity of a single particle in quiescent liquid (m/s)
U_d	particle circulating rate (m/s)
U_g	gas superficial velocity (m/s)
U_l	liquid superficial velocity (m/s)
U_{lc}	liquid superficial velocity in the liquid–solid mixture (m/s)
W_{st}	power consumption for suspending and transporting in unit bed volume
ε_{lc}	liquid holdup in the liquid–solid mixture (εsc =1- εlc)
ε_{lw}	liquid holdup in the primary bubble wake (εsw =1- εlw)
ε_s	solid holdup, εs = (1 -*f*g -*f*w)εsc + *f*wεsw
Λ	specific area (m−1)
Z	local energy dissipation rate per unit mass of liquid
r_p	Mean porous radius

References

1) Weiguo Yang, Jinfu Wang, Tiefeng Wang, Yong Jin (Nov 1999), Experimental study on gas–liquid interfacial area and mass transfer coefficient in three-phase circulating fluidized beds, Chemical Engineering Journal 84 (2001), 485– 49

2) Jiasen Song, Caroline L. Hyndman, Rajesh K. Jakher, Kelly Hamilton, (1999), Fundamentals of hydrodynamics and mass transfer in a three-phase fluidized bed system, Chemical Engineering Science 54 (1999) 4967-4973

3) Weiguo Yang, Jinfu Wang, Liming Zhou, Yong Jin, (1999), Gas-liquid mass transfer behavior in three-phase CFB reactors, Chemical Engineering Science 54 (1999) 5523-5528

4) G.K.Roy, B.C. Meikap , (1997), Removal of phenolic compounds industrial waste water by semifluidized bed bioreactor, Journal of the IPHE ,India, Vol: 1997, No. 3

5) Faical Larachi, Miran cassanello,Andre Laurent,Gabriel Wild ,(1997), Gas-liquid interfacial areas in three phase fixed bed reactors, Chemical Engineering and processing 36, 1997,497-504.

6) S. Maalej, B. Benaddab, M. Otterbein , (2003), Interfacial area and volumetric mass transfer coefficient in a bubble reactor at elevated pressures, Chemical Engineering Science 58 (2003) 2365 – 2376

7) Chong Zheng, Zumao Chen, Yuanding Feng and Hanns Hofmann, (1994), Mass transfer in different flow regimes of three-phase fluidized beds, Chemical Engineering science, vol. 50, no. 10, pp. 1571-1578, 1995

8) G.K.Roy, J.S.N.Murthy ,(1986), Semifluidization a review , Indian chemical engineers, vol.: XXIX No.2, 9-22

9) Mingyan Liu, Jinghai Li, Mooson Kwauk, Application ofthe energy-minimization multi-scale method to gas–liquid–solid fluidized beds, Chemical Engineering Science 56 (2001) 6805–6812

10) Jinghai Li, The EMMS model its application, development and updated concepts , Chemical Engineering Science 54 (1999) 5409}5425

11) Wei Ge, Analytical multi-scale method for multi-phase complex systems in process engineering-Bridging reductionism and holism , Chemical Engineering Science 62 (2007) 3346 – 3377

12) S. Grevskott B.H. Sannes M.P. Dudukovid ; Liquid circulation , bubble size distribution , and solids movement in two- and three-phase bubble columns Chemical Engineering Science, Vol. 51, No. 10, pp. 1703--1713, 1996

13) Guangwen Xu and Jinghai Li ; Analytical solution of the energy minimization multi-scale model for gas- solid two-phase flow , Chemical Engineering Science, Vol. 53, No. 7, pp. 1349Ð1366, 1998

14) Y. Li, G.Q. Yang, J.P. Zhang, L.-S. Fan, Numerical studies of bubble formation dynamics in gas–liquid–solid fluidization at high pressures , Powder Technology 116 (2001) 246–260

15) Jack T. Cornelissena, Fariborz , CFD modelling of a liquid–solid fluidized bed , Chemical Engineering Science 62 (2007) 6334 – 6348

16) Tiefeng Wang, Jinfu Wang , Bubble behavior in gas–liquid–solid three-phase circulating fluidized beds, Chemical Engineering Journal 84 (2001) 397–404

17) Waing, Yu, Li The phase holdups in Gas-Liquid-Solid circulating fluidized bed. Chemical enginereering journal 58, (1995)260

18) Ning Yang, Wei Wang ; Modeling of meso scale structures in particle fluid systems: The EMMS CFD approach, China Particuoogy Vol. 3, Nos. 1-2, 78-79, 2005

19) Bona Lua,b,WeiWanga, Jinghai Lia , Multi-scale CFD simulation of gas–solid flow in MIP reactors with a structure-dependent drag model , Chemical Engineering Science 62 (2007) 5487 – 5494

20) Jinghai Li, Mooson Kwauk , Exploring complex systems in chemical engineering – the multi-scale methodology , Chemical Engineering Science 58 (2003) 521 – 535

21) Jiayuan Zhang,Wei Ge Jinghai Li, Simulation of heterogeneous structures and analysis of energy consumption in particle–fluid systems with pseudo-particle modeling Chemical Engineering Science 60 (2005) 3091 – 3099

22) Y. Li, G.Q. Yang, J.P. Zhang, L.-S. Fan , Numerical studies of bubble formation dynamics in gas–liquid–solid fluidization at high pressures, Powder Technology 116(2001) .246–260

23) Yong Li, Jianping Zhang, Liang-Shih Fan , Numerical simulation of gas-liquid-solid fluidization systems using a combined CFD-VOF-DPM method: bubble wake behavior Chemical Engineering Science 54 (1999) 5101-5107

24) Wei Ge, Jinghai Li, Physical mapping of fluidization regimes -the EMMS approach Chemical Engineering Science 57 (2002) 3993 – 4004

25) Y.T. Shah, D. Gidaspow and D.T. Wawan , Sedimentation of Fine Particles in Nonaqueous Media Part I – Experimental Part II – Modeling ; Colloids and Surfaces, 21 (1986) 393-429

26) C.N. Lim, M.A. Gilbertson, A.J.L. Harrison, Bubble distribution and behavior in bubbling fluidized beds, Chemical Engineering Science 62 (2007) 56 – 69

27) Rupesh K. Reddy, Jyeshtharaj B. Joshi, CFD modeling of pressure drop and drag coefficient in fixed and expanded beds, chemical engineering research and design 86 (2008) 444- 453

28) N.N. Bobkov and YD.P. Gdpalo, The effect of bubble coalescence on mass transfer in fluidized bed. , U.S.S.R., Vol.48, NO.5, 1984, 567-574,

29) Ryszard Pohorecki, Effectiveness of interfacial area for mass transfer in two-phase flow in micro reactors; Chemical Engineering Science 62 (2007) 6495 – 6498

30) Anand A.Samuel V.N.Vedamurthy; mathematical modeling of heat and mass transfer in three phase fluidized bed systems.Math1 Comput. Modelling. Vol. 14, pp. 837-841, 1990

31) Z. Al-Qodaha;_, M. Al-Hassan , Phase holdup and gas-to-liquid mass transfer coefficient in magneto stabilized G-L-S airlift fermenter, Chemical Engineering Journal 79 (2000) 41–52

32) Sang Done Kim and Yong Kang, Heat and mass transfer in three-phase fluidized-bed reactors--an overview ; Chemical engineering science Vol: 52 p3639

33) P.J. Witt , J.H. Perry , M.P. Schwarz , A numerical model for predicting bubble formation in a 3D fluidized bed Applied Mathematical Modeling 22 (1998) 1071 – 1080

34) L.S.Fan; Semi-fluidization : Mass transfer in semi-fluidized bed .A.I.Ch.E Journal (1959)p 407

35) K.Baburao, L.K, Dorisawamy ; A generalized equation for solids distribution in the semi-fluidized MT reactor , A.I.Ch.E journal

36) G.K.Roy, P.SenGupta , prediction of packed bed height in gas-solid semi-fluidization; Ind. Eng. Chem,. Process Des. Develop Vol. 13, No 3, 1974, 221

37) J.M. Begovich, J.S. Watson, Hydrodynamic Characteristics of Three-Phase Fluidized Beds, Fluidization, University Press, Cambridge, 1978, pp. 190–195.